A GENERALIZED MAC SCHEME ON CURVILINEAR DOMAINS

YIN-LIANG HUANG[*], JIAN-GUO LIU[†], AND WEI-CHENG WANG[‡]

Abstract. We propose a simple finite difference scheme for Navier-Stokes equations in primitive formulation on curvilinear domains. With proper boundary treatment and interplay between covariant and contra-variant components, the spatial discretization admits exact Hodge decomposition and energy identity. As a result, the pressure can be decoupled from the momentum equation with explicit time stepping. No artificial pressure boundary condition is needed. In addition, it can be shown that this spatially compatible discretization leads to uniform inf-sup condition, which plays a crucial role in the pressure approximation of both dynamic and steady state calculations. Numerical experiments demonstrate the robustness and efficiency of our scheme.

1. Introduction. In the numerical computation of the Navier-Stokes equation

$$\boldsymbol{u}_t + (\boldsymbol{u} \cdot \nabla)\boldsymbol{u} + \nabla p = \nu \nabla^2 \boldsymbol{u} + \boldsymbol{f} \quad \text{in } \Omega \tag{1.1}$$

$$\nabla \cdot \boldsymbol{u} = 0 \quad \text{in } \Omega \tag{1.2}$$

$$\boldsymbol{u} = \boldsymbol{0} \quad \text{on } \Gamma \tag{1.3}$$

one of the key issue is the proper implementation of boundary conditions. Since the pressure p is not described by an evolutionary equation, one could instead, treat it as a Lagrangian multiplier to enforce the discrete divergence free constraint. To realize it in discrete setting, the discrete gradient, curl and divergence operators are required to satisfy certain compatibility conditions so that the the discrete Hodge decomposition can be performed exactly and efficiently. This is key to decoupling the pressure from the momentum equation and efficiency of the scheme for time dependent problems. In this approach, the pressure is no longer solved via an elliptic PDE and there is no boundary condition involved for the pressure. The classical Mark-And-Cell (MAC) scheme [Le, DHSW, HW] can be interpreted as a typical example of this approach [An].

Inspired by the classical MAC scheme, we propose here a generalized MAC (GMAC) scheme on curvilinear coordinate that preserves the desired properties. This is done by careful construction of appropriate 2nd order finite difference operators such that the differential identities such as

$$\text{curl} \circ \text{grad} \equiv \boldsymbol{0}, \qquad \text{div} \circ \text{curl} \equiv 0 \tag{1.4}$$

remain valid in the discrete setting. In particular, the discrete Hodge decomposition for vector fields can be performed *exactly* and the corresponding linear system for the pressure is symmetric and semi-definite. No pressure boundary condition is needed. The scheme is finite difference in nature and easy to implement on curvilinear domains with simple geometry. Overall, the resulting scheme is robust and efficient as demonstrated by our numerical examples.

The exact Hodge decomposition also leads to a very simple error analysis for the velocity field [HLW]. Rigorous error analysis for the classical MAC scheme was first obtained in [HoW] and for MAC-like schemes on Cartesian grids in [We]. The proof in [HoW, We] is based on high order Strang's expansion. In contrast, the argument in [HLW] explores on the special structure of the spatial discretization and makes use of both the stream function and the discrete analogue of the differential identities (1.4). As a result, an optimal $O(h^2)$ error estimate is obtained provided the exact velocity is in C^4 and pressure in C^3. This may be the minimal regularity requirement in finite difference setting.

---

[*]Department of Applied Mathematics, National University of Tainan, Tainan, 700, Taiwan. (`liang@mail.nutn.edu.tw`)

[†]Department of Physics and Department of Mathematics, Duke University, Durham, NC 27708, USA (`jian-guo.liu@duke.edu`)

[‡]Department of Mathematics, National Tsing Hua University and National Center of Theoretical Sciences, HsinChu, 300, Taiwan. (`wangwc@math.nthu.edu.tw`)

In addition to exact discrete Hodge decomposition, compatibility among spatial discretizations is closely related to the pressure error. The heart of this matter is widely known as the inf-sup condition or Ladyzhenskaya-Babuška-Brezzi (LBB) condition (see (3.74) below). Spatial discretizations that do not satisfy the inf-sup condition usually result in degradation of the accuracy in pressure. This is well documented for steady state ([BS]) and dynamic calculations (see for example [We]). A well known example is the $Q_1 - P_0$ element, with LBB constant $\beta_h = O(h)$, ([BN]). In contrast, GMAC is staggered and supported the same way as the $Q_1 - P_0$ element (and a few other finite difference schemes that fail to satisfy the inf-sup condition), except GMAC results in a different 9-point differencing formula for the viscous term. Nevertheless, it can be shown ([HLW]) that GMAC admits uniform LBB estimate with an $O(1)$ lower bound for smooth grids in 2D. We also give strong numerical evidence for this assertion. See section 3.5 and section 4 for details.

Related works on finite difference and finite volume methods on mapped grids include those designed for NSE in primitive variables on non-staggered or fully staggered curvilinear grids [ZSK, GeS, LB, TC]. See also [NC, CDHM, Ar, ArL, LWa, HS] for numerical methods in curvilinear coordinates on NSE with vorticity-stream formulation, convection-diffusion equation, and other linear equations. In addition, a vast amount of research works have contributed to the development of computational incompressible flows in many aspects. For example, parallel implementation on large scale simulation [OOB, KK], adaptive refinement techniques [ABCHW, RBLCB], fast iterative methods [ESW], multigrid methods [BHM, TOS] and domain decomposition [TW]. For an overview on recent development in CFD, see for example [DFM, GS, KS, FP] and the references therein.

The rest of the paper is organized as follows. In section 2, we review the classical MAC scheme, the boundary treatment and discrete Hodge decomposition. In section 3, we describe our generalized MAC scheme (GMAC) in curvilinear coordinates. The velocity components are located on the same location for convenience in both programming and applications. Representation of the Navier Stokes equation in a 'skewed' local coordinate leads to a natural discretization that gives rise to desired crucial discrete identities. One of the key issue here is to incorporate the boundary conditions into the finite difference operators so that exact summation by parts identity holds. The key properties of MAC scheme and exact discrete Hodge decomposition mentioned above is retained here even for the non-homogeneous boundary conditions. The 3D version of our scheme, as well as possible variants are documented in the appendix. Finally, we perform a systematic numerical test and report the results in section 4.

2. Classical MAC Scheme, Energy Identity and Hodge Decomposition. In this section, we review the classical MAC scheme and fundamental discrete identities associated with it. We first recall the essential ingredients that lead to the energy estimate and the well-posedness of the Navier-Stokes equation (1.1-1.3). Take the inner product with $\boldsymbol{u}$ on both sides of (1.1) and then integrate over Ω using the following facts,

(2.1) $\qquad\qquad\qquad \langle \boldsymbol{u}, \nabla p \rangle = -\langle \nabla \cdot \boldsymbol{u}, p \rangle,$

(2.2) $\qquad\qquad\qquad$ The vector Laplacian ∇^2 is symmetric and non-positive,

(2.3) $\qquad\qquad\qquad \langle N(\boldsymbol{u}), \boldsymbol{u} \rangle = 0,$

where $N(\boldsymbol{u}) = \boldsymbol{u} \cdot \nabla \boldsymbol{u}$ and $\langle \boldsymbol{u}, \boldsymbol{v} \rangle = \int_\Omega \boldsymbol{u} \cdot \boldsymbol{v} \, dx$. It is easy to obtain the basic energy estimate (for $\boldsymbol{f} \equiv \boldsymbol{0}$):

(2.4) $$\frac{1}{2} \frac{d}{dt} \|\boldsymbol{u}\|^2 + \nu \|\nabla \boldsymbol{u}\|^2 = 0.$$

It is therefore desirable if a numerical scheme can preserve discrete analogue of (2.1-2.3) and therefore guarantee the stability of the scheme. A well known example satisfying (2.1, 2.2) is the classical Mark-and-Cell (MAC) scheme [Le, DHSW, HW], where the pressure and the components of the velocity field are placed on staggered grids in such a way that 2nd order centered difference, divergence free constraint

and no-slip, no-penetration boundary conditions all fit naturally and elegantly with the placement of the variables (Figure 2.1).
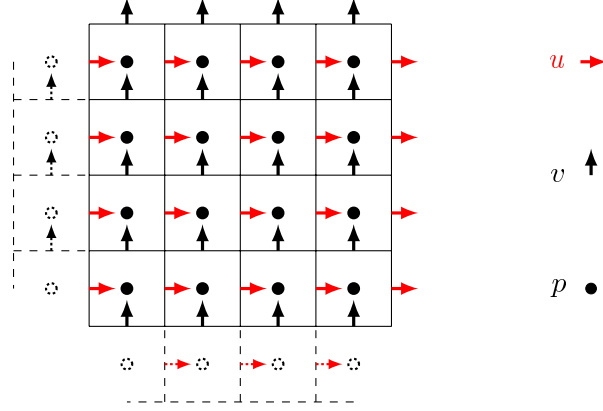

FIG. 2.1. *The MAC grid.*

The fully discrete MAC scheme with explicit treatment for the viscous term is given by:

$$(2.5) \qquad \begin{cases} \dfrac{\boldsymbol{u}^{n+1} - \boldsymbol{u}^n}{\Delta t} + N_h(\boldsymbol{u}^n) + \nabla_h p^{n+1} = \nu \nabla_h^2 \boldsymbol{u}^n + \boldsymbol{f}^n & \text{on } `\rightarrow' \text{ and } `\uparrow', \\[2mm] \nabla_h \cdot \boldsymbol{u}^{n+1} = 0 & \text{on } `\bullet', \\[2mm] \boldsymbol{u}^{n+1} = \boldsymbol{0} & \text{on } \Gamma. \end{cases}$$

The MAC scheme (2.5) is to be completed with extensions on the ghost points outside the computational domain (for example, on the left of $i = 0$),

$$(2.6) \qquad v_{-\frac{1}{2},j}, \quad p_{-\frac{1}{2},j-\frac{1}{2}}.$$

The ghost values in (2.6) are needed to enforce the tangential component of no-slip boundary condition, to evaluate the viscous term and nonlinear term near the boundary, and to impose artificial pressure boundary condition, which is the central issue in pressure Poisson formulation and the key to decoupling the pressure from the momentum equation.

Alternatively, the staggered placement of the variables offers an equivalent interpretation of (2.5) without resorting to the ghost values and artificial pressure boundary condition. This is realized by introducing the 'reduced' operator (c.f. Anderson [An]) that retains a fraction of the original finite difference operators and incorporates the no-slip condition on the boundary grids.

Using the reduced operators (denoted as primed operators), one can recast (2.5) as

$$(2.7) \qquad \begin{cases} \dfrac{\boldsymbol{u}^{n+1} - \boldsymbol{u}^n}{\Delta t} + N_h(\boldsymbol{u}^n) + \nabla_h' p^{n+1} = \nu \nabla_h^{2\prime} \boldsymbol{u}^n + \boldsymbol{f}^n & \text{on } `\rightarrow' \text{ and } `\uparrow', \\[2mm] \nabla_h' \cdot \boldsymbol{u}^{n+1} = 0 & \text{on } `\bullet', \end{cases}$$

Note that in (2.7), the system in self-contained. The ghost values (2.6) are no longer needed. One can therefore identify the pressure gradient as discrete Hodge projection of the acceleration terms onto the orthogonal complement of the divergence free subspace,

$$(2.8) \qquad \frac{\boldsymbol{u}^{n+1}}{\Delta t} + \nabla_h' p^{n+1} = \frac{\boldsymbol{u}^n}{\Delta t} - N_h(\boldsymbol{u}^n) + \nu \nabla_h^{2\prime} \boldsymbol{u}^n + \boldsymbol{f}^n, \quad \nabla_h' \cdot \boldsymbol{u}^{n+1} = 0.$$

3

Moreover, the pressure can be easily decoupled from (2.8). No artificial pressure boundary condition is needed (the curvilinear analogue of the reduced operators and aforementioned properties will be explained in section 3.2 and therefore not detailed here). The resulting scheme is robust and efficient. However, the restriction of Cartesian grids have limited the applicability and popularity of the MAC scheme. In addition, issues of high order time discretization and cell Reynolds number constraint have raised controversy and were not fully understood until the 90's [EL]. In (2.5), we have illustrated these issues using first order forward Euler discretization. Proper high order time-discretization and its connection with the cell Reynolds number can be found in [EL].

Motivated by the success of the MAC scheme, we propose in this work a second order finite difference scheme for Navier-Stokes equation on curvilinear domains. The velocity field and pressure are placed on cell centers and grid points respectively. With a set of 'skewed' coordinates, the Navier-Stokes equation can be discretized naturally in such a way that the discrete analogue of (2.1-2.3) remain valid. As a consequence, the resulting scheme admits a discrete energy estimate. In addition, the scheme also preserves the vector identities (1.4) in discrete settings. This is key to discrete Hodge decomposition and plays an essential role in the efficiency, as well as rigorous error analysis of our scheme.

Another appealing feature of the MAC scheme is about the following generalized Stokes system ($\alpha \geq 0$):

$$(2.9) \qquad \begin{cases} (\alpha - \nabla_h^{2\prime})\boldsymbol{u} + \nabla_h'p = \boldsymbol{f} & \text{on '$\rightarrow$' and '$\uparrow$',} \\ \nabla_h' \cdot \boldsymbol{u} = 0 & \text{on '$\bullet$',} \end{cases}$$

Equation (2.9) arises naturally from steady state calculation or partially implicit time stepping for the Navier-Stokes equation on MAC grid. The solvability of (2.9) and uniform bound of the solution operator are direct consequences of the LBB condition. The verification of the LBB condition is vital to pressure error estimate for both static and dynamic problems and is a long-standing open problem for MAC scheme. In [HWu], the authors constructed a new finite element method for the Stokes system based on three sets of tessellation of rectangular cells. The resulting scheme combined with quadrature formulas corresponds to the classical MAC scheme (2.9) equipped with the Orszag-Israeli vorticity boundary condition [OI] (see also [EL], Table I):

$$(2.10) \qquad u_{0,j+\frac{1}{2}} = 0, \quad v_{-\frac{1}{2},j} = -2v_{\frac{1}{2},j} + \tfrac{1}{3}v_{\frac{3}{2},j},$$

and satisfies uniform LBB estimate. This method is later extended to NSE in [HY]. The issue of uniform LBB estimate for MAC scheme with the original reflection boundary condition, $v_{-\frac{1}{2},j} = -v_{\frac{1}{2},j}$, will be addressed in a forthcoming paper. An alternative approach for the pressure error estimate on MAC scheme using high order Strang's expansion can be found in [HW].

3. Generalized MAC Scheme on Curvilinear Domains. The generalized MAC scheme is based on discretizing Navier-Stokes equation in rotational form:

$$(3.1) \qquad \begin{array}{rcl} \boldsymbol{u}_t + \boldsymbol{\omega} \times \boldsymbol{u} + \nabla p & = & -\nu\nabla \times \boldsymbol{\omega} + \boldsymbol{f} \\ \boldsymbol{\omega} & = & \nabla \times \boldsymbol{u} \qquad \text{in } \Omega \\ \nabla \cdot \boldsymbol{u} & = & 0 \\ \boldsymbol{u} & = & \boldsymbol{0} \qquad \text{on } \Gamma \end{array}$$

On a curvilinear domain, we place all three components of the velocity on cell centers $\boldsymbol{x}(\xi_{i+\frac{1}{2}}^1, \xi_{j+\frac{1}{2}}^2, \xi_{k+\frac{1}{2}}^3)$, while the pressure and the vorticity components are placed on the grid points $\boldsymbol{x}(\xi_i^1, \xi_j^2, \xi_k^3)$. Here (ξ^1, ξ^2, ξ^3) is the coordinate in the computational domain and $\boldsymbol{x}$ is the position vector in physical domain Ω.

In addition to generalization to curvilinear coordinates, GMAC differs from the classical MAC scheme in the placement of the velocity components. One advantage of placing all three components of velocity at the same place is that (2.3) can be naturally realized in the discrete setting. Together with other vector
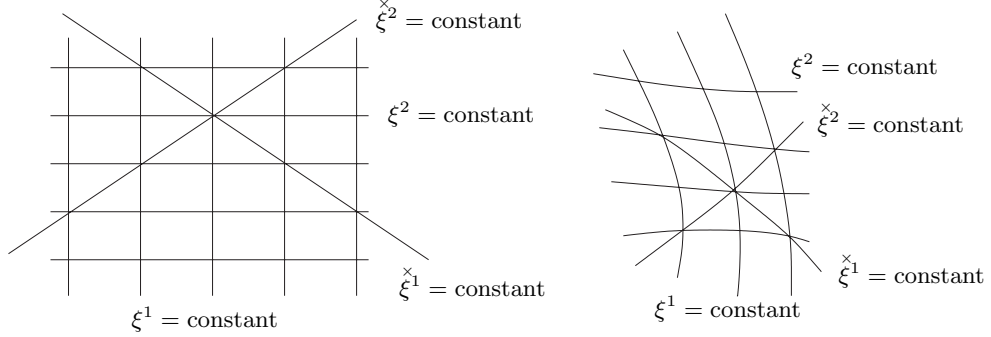
4

FIG. 3.1. *The computational domain (left) and the physical domain (right).*

identities, this ensures the stability of GMAC. More importantly, the resulting discrete Laplacian for p is self-adjoint and non-positive definite as long as the cells are non-singular, regardless of the regularity of the grids. See the discussion in section 3.4. For the fully staggered case, where different components of $\boldsymbol{u}$ are placed on different positions as in the classical MAC case, positivity of the pressure equation on curvilinear domains may require extra assumption on smoothness of the grids ([BD], p147-150).

For simplicity of presentation, we start with the 2D case:

$$
\begin{aligned}
\boldsymbol{u}_t + \omega \boldsymbol{u}^\perp + \nabla p &= \nu \nabla^\perp \omega + \boldsymbol{f} \\
\omega &= \nabla^\perp \cdot \boldsymbol{u} \qquad && \text{in } \Omega \\
\nabla \cdot \boldsymbol{u} &= 0 \\
\boldsymbol{u} &= \boldsymbol{0} \qquad && \text{on } \Gamma
\end{aligned}
$$

(3.2)

The discretization of (3.2) and boundary treatment in curvilinear coordinate will be explained in detail in following subsections.

3.1. Differential operators in curvilinear coordinate. In the 2D case, $\boldsymbol{x} = (x, y)$ is the position vector in the physical domain and (ξ^1, ξ^2) the coordinate in the computational domain with mesh size $\Delta \xi^1 = h_1$ and $\Delta \xi^2 = h_2$. We further introduce a new set of coordinates in the skewed direction by

$$
\overset{\times}{\xi}^1 := \frac{h_2 \xi^1 + h_1 \xi^2}{\sqrt{h_1^2 + h_2^2}}, \qquad \overset{\times}{\xi}^2 := \frac{-h_2 \xi^1 + h_1 \xi^2}{\sqrt{h_1^2 + h_2^2}}.
$$

(3.3)

as illustrated in Figure 3.1.

Once the a local coordinate is chosen, the intrinsic differential operators can be determined following standard procedure. Through out this paper, we use '$\times$' to emphasis that the corresponding quantities are computed in the skewed variables $\overset{\times}{\xi}{}^\alpha$. Denote by

$$
\begin{aligned}
\overset{\times}{\boldsymbol{e}}_1 &= \frac{\partial \boldsymbol{x}}{\partial \overset{\times}{\xi}^1}, \qquad \overset{\times}{\boldsymbol{e}}_2 = \frac{\partial \boldsymbol{x}}{\partial \overset{\times}{\xi}^2}, \\
\overset{\times}{\boldsymbol{e}}{}^1 &= \nabla \overset{\times}{\xi}^1, \qquad \overset{\times}{\boldsymbol{e}}{}^2 = \nabla \overset{\times}{\xi}^2,
\end{aligned}
$$

(3.4)

the metric tensors with respect to the skewed coordinate $(\overset{\times}{\xi}^1, \overset{\times}{\xi}^2)$ is then given by

$$
\overset{\times}{g}{}^{\mu\nu} = \overset{\times}{\boldsymbol{e}}{}^\mu \cdot \overset{\times}{\boldsymbol{e}}{}^\nu, \qquad \overset{\times}{g}_{\mu\nu} = \overset{\times}{\boldsymbol{e}}_\mu \cdot \overset{\times}{\boldsymbol{e}}_\nu, \qquad \mu, \nu = 1, 2.
$$

(3.5)

and

$$
\overset{\times}{g} := \det(\overset{\times}{g}_{\mu\nu}).
$$

(3.6)

5

The following identities follow immediately from definition:

$$(3.7) \qquad\qquad \sqrt{\overset{\times}{g}} = \det\left(\frac{\partial \boldsymbol{x}}{\partial \overset{\times}{\boldsymbol{\xi}}}\right)$$

$$(3.8) \qquad\qquad \sum_{\gamma=1}^{2} \overset{\times}{g}^{\mu\gamma}\overset{\times}{g}_{\gamma\nu} = \delta^{\mu}_{\nu}.$$

We use $(\overset{\times}{u}_1, \overset{\times}{u}_2)$ and $(\overset{\times}{u}^1, \overset{\times}{u}^2)$ to denote the covariant and contra-variant components of a vector field $\boldsymbol{u}$ in the $\overset{\times}{\xi}^{\alpha}$ coordinate:

$$\boldsymbol{u} = \overset{\times}{u}^1 \overset{\times}{\boldsymbol{e}}_1 + \overset{\times}{u}^2 \overset{\times}{\boldsymbol{e}}_2 = \overset{\times}{u}_1 \overset{\times}{\boldsymbol{e}}^1 + \overset{\times}{u}_2 \overset{\times}{\boldsymbol{e}}^2.$$

The transformation between co-variant and contra-variant components is given by

$$(3.9) \qquad \overset{\times}{u}^{\mu} = \sum_{\gamma=1}^{2} \overset{\times}{g}^{\mu\gamma}\overset{\times}{u}_{\gamma}, \qquad \overset{\times}{u}_{\nu} = \sum_{\gamma=1}^{2} \overset{\times}{g}_{\gamma\nu}\overset{\times}{u}^{\gamma}, \qquad \mu, \nu = 1, 2.$$

We summarize relevant formulae for (3.2) as follows:

$$\nabla p = \frac{\partial p}{\partial \overset{\times}{\xi}^1}\overset{\times}{\boldsymbol{e}}^1 + \frac{\partial p}{\partial \overset{\times}{\xi}^2}\overset{\times}{\boldsymbol{e}}^2,$$

$$\nabla^{\perp}\omega = \frac{1}{\sqrt{\overset{\times}{g}}}\left(-\frac{\partial \omega}{\partial \overset{\times}{\xi}^2}\overset{\times}{\boldsymbol{e}}_1 + \frac{\partial \omega}{\partial \overset{\times}{\xi}^1}\overset{\times}{\boldsymbol{e}}_2\right),$$

$$\nabla \cdot \boldsymbol{u} = \frac{1}{\sqrt{\overset{\times}{g}}}\left(\frac{\partial}{\partial \overset{\times}{\xi}^1}(\sqrt{\overset{\times}{g}}\,\overset{\times}{u}^1) + \frac{\partial}{\partial \overset{\times}{\xi}^2}(\sqrt{\overset{\times}{g}}\,\overset{\times}{u}^2)\right),$$

$$\nabla^2 p = \nabla \cdot \nabla p = \frac{1}{\sqrt{\overset{\times}{g}}}\sum_{\mu,\nu=1}^{2}\frac{\partial}{\partial \overset{\times}{\xi}^{\mu}}\left(\sqrt{\overset{\times}{g}}\,\overset{\times}{g}^{\mu\nu}\frac{\partial p}{\partial \overset{\times}{\xi}^{\nu}}\right),$$

$$\boldsymbol{u}^{\perp} = \sqrt{\overset{\times}{g}}(-\overset{\times}{u}^2\overset{\times}{\boldsymbol{e}}^1 + \overset{\times}{u}^1\overset{\times}{\boldsymbol{e}}^2) = \frac{1}{\sqrt{\overset{\times}{g}}}(-\overset{\times}{u}_2\overset{\times}{\boldsymbol{e}}_1 + \overset{\times}{u}_1\overset{\times}{\boldsymbol{e}}_2),$$

$$\omega = \nabla^{\perp}\cdot \boldsymbol{u} = \frac{1}{\sqrt{\overset{\times}{g}}}\left(\frac{\partial \overset{\times}{u}_2}{\partial \overset{\times}{\xi}^1} - \frac{\partial \overset{\times}{u}_1}{\partial \overset{\times}{\xi}^2}\right).$$

Whenever necessary, the co-variant and contra-variant components can be converted to each other using (3.9). For example,

$$\nabla p = \left(\frac{\partial p}{\partial \overset{\times}{\xi}^1}\overset{\times}{g}^{11} + \frac{\partial p}{\partial \overset{\times}{\xi}^2}\overset{\times}{g}^{21}\right)\overset{\times}{\boldsymbol{e}}_1 + \left(\frac{\partial p}{\partial \overset{\times}{\xi}^1}\overset{\times}{g}^{12} + \frac{\partial p}{\partial \overset{\times}{\xi}^2}\overset{\times}{g}^{22}\right)\overset{\times}{\boldsymbol{e}}_2.$$

3.2. Spatial Discretization. The choice of the skewed coordinate in motivated by the jump condition capturing scheme developed for elliptic interface problems [Wa]. It was shown that, using the skewed coordinate as independent variables, the interface jump conditions can be naturally incorporated into the

finite difference operator. The resulting scheme is symmetric, definite and second order accurate even when the diffusion coefficient has a jump continuity across the material interface.

We now give detailed description on the spatial discretization of our scheme, starting with the metric tensor. In case the coordinate mapping $(\xi^1, \xi^2) \mapsto (x, y)$ is explicitly given, one can compute the metric tensors from (3.4)-(3.8) and use it in the discretizations (3.30)-(3.36) below. Alternatively, one can also compute the numerical metric tensors $\overset{\times}{g}{}^h_{\alpha\beta}$ from straightforward centered difference:

$$(\overset{\times}{g}{}^h_{11})_{i+\frac{1}{2},j+\frac{1}{2}} := \frac{\boldsymbol{x}_{i+1,j+1} - \boldsymbol{x}_{i,j}}{\overset{\times}{h}} \cdot \frac{\boldsymbol{x}_{i+1,j+1} - \boldsymbol{x}_{i,j}}{\overset{\times}{h}},$$

$$(\overset{\times}{g}{}^h_{22})_{i+\frac{1}{2},j+\frac{1}{2}} := \frac{\boldsymbol{x}_{i,j+1} - \boldsymbol{x}_{i+1,j}}{\overset{\times}{h}} \cdot \frac{\boldsymbol{x}_{i,j+1} - \boldsymbol{x}_{i+1,j}}{\overset{\times}{h}},$$

$$(\overset{\times}{g}{}^h_{12})_{i+\frac{1}{2},j+\frac{1}{2}} = (\overset{\times}{g}{}^h_{21})_{i+\frac{1}{2},j+\frac{1}{2}} := \frac{\boldsymbol{x}_{i+1,j+1} - \boldsymbol{x}_{i,j}}{\overset{\times}{h}} \cdot \frac{\boldsymbol{x}_{i,j+1} - \boldsymbol{x}_{i+1,j}}{\overset{\times}{h}}.$$

where

(3.10)
$$\overset{\times}{h} := \frac{2h_1 h_2}{\sqrt{h_1^2 + h_2^2}} = \Delta \overset{\times}{\xi}{}^1 = \Delta \overset{\times}{\xi}{}^2$$

is the mesh size in the skewed directions $\overset{\times}{\xi}{}^1$ and $\overset{\times}{\xi}{}^2$. Note that the indices i, j refer to the ξ variables, not the $\overset{\times}{\xi}$ ones.

The numerical contra-variant components (3.8) are defined through analogue of (3.8):

$$(\overset{\times}{g}{}^{\alpha\beta}_h) := (\overset{\times}{g}{}^h_{\mu\nu})^{-1}$$

that is

$$\sum_{\lambda=1}^{2} \overset{\times}{g}{}^{\mu\lambda}_h \overset{\times}{g}{}^h_{\lambda\nu} = \delta^\mu_\nu.$$

The numerical Jacobian on cell centers and grids are given by

$$\overset{\times}{g}_{h\,i+\frac{1}{2},j+\frac{1}{2}} := \det \begin{pmatrix} \overset{\times}{g}{}^h_{11} & \overset{\times}{g}{}^h_{12} \\ \overset{\times}{g}{}^h_{21} & \overset{\times}{g}{}^h_{22} \end{pmatrix}_{i+\frac{1}{2},j+\frac{1}{2}}$$

and

$$\sqrt{\overset{\times}{g}_h}_{i,j} := \frac{1}{4}\left(\sqrt{\overset{\times}{g}_h}_{i+\frac{1}{2},j+\frac{1}{2}} + \sqrt{\overset{\times}{g}_h}_{i+\frac{1}{2},j-\frac{1}{2}} + \sqrt{\overset{\times}{g}_h}_{i-\frac{1}{2},j+\frac{1}{2}} + \sqrt{\overset{\times}{g}_h}_{i-\frac{1}{2},j-\frac{1}{2}} \right).$$

Next, we introduce the discrete grad, div, curl and Laplacian. With the semi-staggered placement of the variables $\boldsymbol{u}$, p and ω as in Figure 3.4, it is straight forward to discretize (3.2) using centered difference. The crucial issue here is the boundary treatment of these operators which plays an essential role in the stability of our scheme. We define the 1D reduced finite difference operator by

(3.11)
$$(D'b)_i := \begin{cases} \frac{b_{\frac{1}{2}} - 0}{\frac{1}{2}h} & i = 0 \\ \frac{b_{i+\frac{1}{2}} - b_{i-\frac{1}{2}}}{h} & 1 \le i \le M - 1 \\ \frac{0 - b_{M-\frac{1}{2}}}{\frac{1}{2}h} & i = M \end{cases}$$

A direct consequence of the reduced differencing is the exact summation by parts identity as observed in [An]:

PROPOSITION 1.

$$(3.12) \qquad h \sum_{i=1}^{M} b_{i-\frac{1}{2}} (Da)_{i-\frac{1}{2}} = -h \sum_{i=0}^{M}{}' a_i (D'b)_i$$

where the primed sum denotes half weight on the boundary:

$$(3.13) \qquad \sum_{i=0}^{M}{}' a_i = \frac{1}{2} a_0 + \sum_{i=1}^{M-1} a_i + \frac{1}{2} a_M.$$

We now introduce the following notations

$$(3.14) \qquad \Omega_{\mathrm{c}} := \left\{ \boldsymbol{x}(\xi^1_{i-\frac{1}{2}}, \xi^2_{j-\frac{1}{2}}) \,|\, 1 \leq i \leq M, \, 1 \leq j \leq N \right\}$$

$$(3.15) \qquad \mathring{\Omega}_{\mathrm{g}} := \left\{ \boldsymbol{x}(\xi^1_i, \xi^2_j) \,|\, 1 \leq i \leq M-1, \, 1 \leq j \leq N-1 \right\}$$

$$(3.16) \qquad \bar{\Omega}_{\mathrm{g}} := \left\{ \boldsymbol{x}(\xi^1_i, \xi^2_j) \,|\, 0 \leq i \leq M, \, 0 \leq j \leq N \right\}$$

$$(3.17) \qquad \Gamma_{\mathrm{g}} := \bar{\Omega}_{\mathrm{g}} \setminus \mathring{\Omega}_{\mathrm{g}}$$

$$(3.18) \qquad \Gamma_{\mathrm{c}} := \left\{ \boldsymbol{x}(\xi^1_{i-\frac{1}{2}}, \xi^2_j) \,|\, 1 \leq i \leq M, \, j = 0, N \right\} \cup \left\{ \boldsymbol{x}(\xi^1_i, \xi^2_{j-\frac{1}{2}}) \,|\, i = 0, M, \, 1 \leq j \leq N \right\}$$

$$(3.19) \qquad \bar{\Omega}_{\mathrm{ge}} := \left\{ \boldsymbol{x}(\xi^1_i, \xi^2_j) \in \bar{\Omega}_{\mathrm{g}} \,|\, i + j \text{ is even} \right\}$$

$$(3.20) \qquad \bar{\Omega}_{\mathrm{go}} := \left\{ \boldsymbol{x}(\xi^1_i, \xi^2_j) \in \bar{\Omega}_{\mathrm{g}} \,|\, i + j \text{ is odd} \right\}$$

and denote by $L^2(\bar{\Omega}_{\mathrm{g}}, \mathbb{R})$ the collection of real valued functions on $\bar{\Omega}_{\mathrm{g}}$ and $L^2(\Omega_{\mathrm{c}}, \mathbb{R}^2)$ the vector fields on Ω_{c}:

$$(3.21) \qquad L^2(\bar{\Omega}_{\mathrm{g}}, \mathbb{R}) := \{\omega : \bar{\Omega}_{\mathrm{g}} \to \mathbb{R}\}$$

$$(3.22) \qquad L^2(\Omega_{\mathrm{c}}, \mathbb{R}) := \{u : \Omega_{\mathrm{c}} \to \mathbb{R}\}$$

$$(3.23) \qquad L^2(\Omega_{\mathrm{c}}, \mathbb{R}^2) := \{\boldsymbol{u} : \Omega_{\mathrm{c}} \to \mathbb{R}^2\}$$

and

$$(3.24) \qquad L^2(\bar{\Omega}_{\mathrm{g}}, \mathbb{R})/\mathbb{R}^2 := \left\{ p \in L^2(\bar{\Omega}_{\mathrm{g}}, \mathbb{R}) \,\Big|\, \sum_{\bar{\Omega}_{\mathrm{ge}}}{}' (\sqrt{\mathring{g}_h} p)_{i,j} = 0 = \sum_{\bar{\Omega}_{\mathrm{go}}}{}' (\sqrt{\mathring{g}_h} p)_{i,j} \right\}$$

$$(3.25) \qquad L^2_c(\bar{\Omega}_{\mathrm{g}}, \mathbb{R}) := \{\psi \in L^2(\bar{\Omega}_{\mathrm{g}}, \mathbb{R}) \,|\, \psi = \text{ constant on each connected component of } \Gamma \}$$

In view of Proposition 1, it is natural to define the reduced difference operator in the skewed variables as

DEFINITION 1.

1. For $a \in L^2(\bar{\Omega}_{\mathrm{g}}, \mathbb{R})$,

$$(3.26) \qquad (\mathring{D}_1 a)_{i-\frac{1}{2}, j-\frac{1}{2}} := \frac{a_{i,j} - a_{i-1,j-1}}{\overset{\times}{h}}, \quad (\mathring{D}_2 a)_{i-\frac{1}{2}, j-\frac{1}{2}} := \frac{a_{i-1,j} - a_{i,j-1}}{\overset{\times}{h}}.$$

2. *For* $b \in L^2(\Omega_c, \mathbb{R})$,

$$(3.27) \qquad (\mathring{D}'_1 b)_{i,j} := \begin{cases} \dfrac{b_{i+\frac{1}{2},j+\frac{1}{2}} - b_{i-\frac{1}{2},j-\frac{1}{2}}}{\overset{\times}{h}} & 0 < i < M,\ 0 < j < N; \\[2ex] \dfrac{b_{\frac{1}{2},j+\frac{1}{2}}}{\frac{1}{2}\overset{\times}{h}} & i = 0,\ 0 < j < N; \\[2ex] \dfrac{b_{\frac{1}{2},\frac{1}{2}}}{\frac{1}{4}\overset{\times}{h}} & (i,j) = (0,0); \\[2ex] 0 & (i,j) = (0,N). \end{cases}$$

$$(3.28) \qquad (\mathring{D}'_2 b)_{i,j} := \begin{cases} \dfrac{b_{i-\frac{1}{2},j+\frac{1}{2}} - b_{i+\frac{1}{2},j-\frac{1}{2}}}{\overset{\times}{h}} & 0 < i < M,\ 0 < j < N; \\[2ex] \dfrac{-b_{\frac{1}{2},j-\frac{1}{2}}}{\frac{1}{2}\overset{\times}{h}} & i = 0,\ 0 < j < N; \\[2ex] 0 & (i,j) = (0,0); \\[2ex] \dfrac{-b_{\frac{1}{2},N-\frac{1}{2}}}{\frac{1}{4}\overset{\times}{h}} & (i,j) = (0,N). \end{cases}$$

Here in Definition 1 and the rest of the paper, we use the prime to indicate that the reduced difference is applied on boundary when the standard finite difference requires grid points outside the computational domain.

The (reduced) finite difference in the $\overset{\times}{\xi}$ variables extends naturally to the discrete grad, div, curl and Laplacian operators as follows:

DEFINITION 2. *For* $a \in L^2(\bar{\Omega}_g, \mathbb{R})$, *we define*

$$(3.29) \qquad \overset{\times}{\nabla}_h : L^2(\bar{\Omega}_g, \mathbb{R}) \mapsto L^2(\Omega_c, \mathbb{R}^2), \qquad \overset{\times}{\nabla}_h a := (\mathring{D}_1 a)\, \overset{\times}{e}^1 + (\mathring{D}_2 a)\, \overset{\times}{e}^2$$

and

$$(3.30) \qquad \overset{\times}{\nabla}_h^{\perp} : L^2(\bar{\Omega}_g, \mathbb{R}) \mapsto L^2(\Omega_c, \mathbb{R}^2), \qquad \overset{\times}{\nabla}_h^{\perp} a := \dfrac{-\mathring{D}_2 a}{\sqrt{\overset{\times}{g}_h}}\, \overset{\times}{e}_1 + \dfrac{\mathring{D}_1 a}{\sqrt{\overset{\times}{g}_h}}\, \overset{\times}{e}_2.$$

DEFINITION 3. *Let* $\boldsymbol{u} = \overset{\times}{u}^1 \overset{\times}{e}_1 + \overset{\times}{u}^2 \overset{\times}{e}_2 \in L^2(\Omega_c, \mathbb{R}^2)$. *We define*

$$(3.31) \qquad \overset{\times}{\nabla}_h' \cdot : L^2(\Omega_c, \mathbb{R}^2) \mapsto L^2(\bar{\Omega}_g, \mathbb{R}), \qquad \overset{\times}{\nabla}_h' \cdot \boldsymbol{u} = \dfrac{1}{\sqrt{\overset{\times}{g}_h}}\Big(\mathring{D}'_1\big(\sqrt{\overset{\times}{g}_h}\, \overset{\times}{u}^1\big) + \mathring{D}'_2\big(\sqrt{\overset{\times}{g}_h}\, \overset{\times}{u}^2\big) \Big)$$

and

$$(3.32) \qquad \overset{\times}{\nabla}_h^{\perp}{}' \cdot : L^2(\Omega_c, \mathbb{R}^2) \mapsto L^2(\bar{\Omega}_g, \mathbb{R}), \qquad \overset{\times}{\nabla}_h^{\perp}{}' \cdot \boldsymbol{u} = \dfrac{1}{\sqrt{\overset{\times}{g}_h}}(\mathring{D}'_1 \overset{\times}{u}_2 - \mathring{D}'_2 \overset{\times}{u}_1).$$
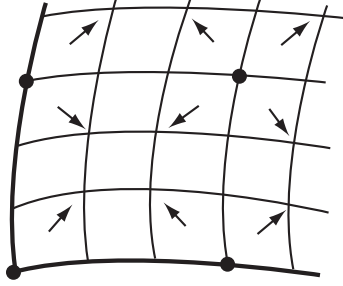
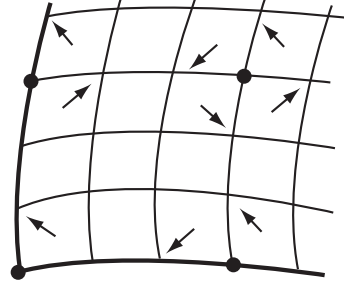FIG. 3.2. *Schematic illustration of* $\breve{\nabla}'_h \cdot \boldsymbol{u}$.

FIG. 3.3. *Schematic illustration of* $\breve{\nabla}_h^{\perp\,\prime} \cdot \boldsymbol{u}$.

The realization of (3.31) *and* (3.32) *on typical interior, boundary and corner points are given by*

$$(3.33) \quad (\overset{\times}{\nabla}'_h \cdot \boldsymbol{u})_{i,j} = \begin{cases} \dfrac{1}{\sqrt{\overset{\times}{g}_{h_{i,j}}}} \left(\dfrac{(\sqrt{\overset{\times}{g}_h}\,\overset{\times}{u}^1)_{i+\frac{1}{2},j+\frac{1}{2}} - (\sqrt{\overset{\times}{g}_h}\,\overset{\times}{u}^1)_{i-\frac{1}{2},j-\frac{1}{2}}}{\overset{\times}{h}} \right. \\ \left. \qquad + \dfrac{(\sqrt{\overset{\times}{g}_h}\,\overset{\times}{u}^2)_{i-\frac{1}{2},j+\frac{1}{2}} - (\sqrt{\overset{\times}{g}_h}\,\overset{\times}{u}^2)_{i+\frac{1}{2},j-\frac{1}{2}}}{\overset{\times}{h}} \right), \quad 0 < i < M,\ 0 < j < N; \\[2ex] \dfrac{2}{\sqrt{\overset{\times}{g}_{h_{0,j}}}} \dfrac{(\sqrt{\overset{\times}{g}_h}\,\overset{\times}{u}^1)_{\frac{1}{2},j+\frac{1}{2}} - (\sqrt{\overset{\times}{g}_h}\,\overset{\times}{u}^2)_{\frac{1}{2},j-\frac{1}{2}}}{\overset{\times}{h}}, \qquad\qquad i = 0,\ 0 < j < N; \\[2ex] \dfrac{4}{\sqrt{\overset{\times}{g}_{h_{0,0}}}} \dfrac{(\sqrt{\overset{\times}{g}_h}\,\overset{\times}{u}^1)_{\frac{1}{2},\frac{1}{2}}}{\overset{\times}{h}}, \qquad\qquad\qquad\qquad (i,j) = (0,0), \end{cases}$$

and

$$(3.34) \quad (\overset{\times}{\nabla}_h^{\perp\,\prime} \cdot \boldsymbol{u})_{i,j} = \begin{cases} \dfrac{1}{\sqrt{\overset{\times}{g}_{h_{i,j}}}} \left(\dfrac{(\overset{\times}{u}_2)_{i+\frac{1}{2},j+\frac{1}{2}} - (\overset{\times}{u}_2)_{i-\frac{1}{2},j-\frac{1}{2}}}{\overset{\times}{h}} \right. \\ \left. \qquad - \dfrac{(\overset{\times}{u}_1)_{i-\frac{1}{2},j+\frac{1}{2}} - (\overset{\times}{u}_1)_{i+\frac{1}{2},j-\frac{1}{2}}}{\overset{\times}{h}} \right), \quad 0 < i < M,\ 0 < j < N; \\[2ex] \dfrac{2}{\sqrt{\overset{\times}{g}_{h_{0,j}}}} \dfrac{(\overset{\times}{u}_2)_{\frac{1}{2},j+\frac{1}{2}} + (\overset{\times}{u}_1)_{\frac{1}{2},j-\frac{1}{2}}}{\overset{\times}{h}}, \qquad\qquad i = 0,\ 0 < j < N; \\[2ex] \dfrac{4}{\sqrt{\overset{\times}{g}_{h_{0,0}}}} \dfrac{(\overset{\times}{u}_2)_{\frac{1}{2},\frac{1}{2}}}{\overset{\times}{h}}, \qquad\qquad\qquad\qquad (i,j) = (0,0). \end{cases}$$

See also Figure 3.2 and Figure 3.3.

Finally, the discrete Laplacian is defined in a similar way (see also [Wa] for the reduced Laplacian in the skewed variables for elliptic interface problems):

DEFINITION 4. *For $a \in L^2(\bar{\Omega}_{\mathrm{g}}, \mathbb{R})$, define*

$$(3.35) \qquad \mathring{\triangle}'_h : L^2(\bar{\Omega}_{\mathrm{g}}, \mathbb{R}) \mapsto L^2(\bar{\Omega}_{\mathrm{g}}, \mathbb{R}), \qquad \mathring{\triangle}'_h a = \frac{1}{\sqrt{\mathring{g}_h}} \sum_{\mu,\nu=1}^{2} \mathring{D}'_\mu (\sqrt{\mathring{g}_h} \mathring{g}_h^{\mu\nu} \mathring{D}_\nu a).$$

That is,

$$(3.36)$$

$$(\mathring{\triangle}'_h a)_{i,j} = \begin{cases} \dfrac{1}{\sqrt{\mathring{g}_{h_{i,j}}}} \left(\dfrac{(\mathring{q}_h^{11} \mathring{D}_1 a + \mathring{q}_h^{12} \mathring{D}_2 a)_{i+\frac{1}{2},j+\frac{1}{2}}}{\mathring{h}} + \dfrac{(\mathring{q}_h^{21} \mathring{D}_1 a + \mathring{q}_h^{22} \mathring{D}_2 a)_{i-\frac{1}{2},j+\frac{1}{2}}}{\mathring{h}} \right. \\[2ex] \qquad \left. - \dfrac{(\mathring{q}_h^{11} \mathring{D}_1 a + \mathring{q}_h^{12} \mathring{D}_2 a)_{i-\frac{1}{2},j-\frac{1}{2}}}{\mathring{h}} - \dfrac{(\mathring{q}_h^{21} \mathring{D}_1 a + \mathring{q}_h^{22} \mathring{D}_2 a)_{i+\frac{1}{2},j-\frac{1}{2}}}{\mathring{h}} \right), \quad \begin{matrix} 0 < i < M \\ 0 < j < N \end{matrix} ; \\[4ex] \dfrac{2}{\sqrt{\mathring{g}_{h_{0,j}}}} \left(\dfrac{(\mathring{q}_h^{11} \mathring{D}_1 a + \mathring{q}_h^{12} \mathring{D}_2 a)_{\frac{1}{2},j+\frac{1}{2}}}{\mathring{h}} - \dfrac{(\mathring{q}_h^{21} \mathring{D}_1 a + \mathring{q}_h^{22} \mathring{D}_2 a)_{\frac{1}{2},j-\frac{1}{2}}}{\mathring{h}} \right), \quad \begin{matrix} i = 0 \\ 0 < j < N \end{matrix} ; \\[4ex] \dfrac{4}{\sqrt{\mathring{g}_{h_{0,0}}}} \dfrac{(\mathring{q}_h^{11} \mathring{D}_1 a + \mathring{q}_h^{12} \mathring{D}_2 a)_{\frac{1}{2},\frac{1}{2}}}{\mathring{h}}, \qquad\qquad\qquad (i,j) = (0,0), \end{cases}$$

where $\mathring{q}_h^{\alpha\beta} = \sqrt{\mathring{g}_h} \mathring{g}_h^{\alpha\beta}$.

We are now ready to state the key Lemma associated with the reduced difference operators. Define the discrete inner products

$$(3.37) \qquad \begin{aligned} \langle \boldsymbol{u} , \boldsymbol{v} \rangle_{\Omega_{\mathrm{c}}} &= h_1 h_2 \sum_{i=0}^{M-1} \sum_{j=0}^{N-1} \left((\boldsymbol{u} \cdot \boldsymbol{v}) \sqrt{g_h} \right)_{i+\frac{1}{2},j+\frac{1}{2}} = h_1 h_2 \sum_{i=0}^{M-1} \sum_{j=0}^{N-1} \left((\mathring{u}_1 \mathring{v}^1 + \mathring{u}_2 \mathring{v}^2) \sqrt{g_h} \right)_{i+\frac{1}{2},j+\frac{1}{2}} \\ &= h_1 h_2 \sum_{i=0}^{M-1} \sum_{j=0}^{N-1} \left(\left(\mathring{u}^1 \mathring{v}_1 + \mathring{u}^2 \mathring{v}_2 \right) \sqrt{g_h} \right)_{i+\frac{1}{2},j+\frac{1}{2}}, \qquad \boldsymbol{u}, \boldsymbol{v} \in L^2(\Omega_{\mathrm{c}}, \mathbb{R}^2). \end{aligned}$$

$$(3.38) \qquad\qquad \langle a , b \rangle_{\bar{\Omega}_{\mathrm{g}}} = h_1 h_2 \sum_{i=0}^{M} {}' \sum_{j=0}^{N} {}' \left(a\, b\, \sqrt{g_h} \right)_{i,j}, \qquad a, b \in L^2(\bar{\Omega}_{\mathrm{g}}, \mathbb{R})$$

and the corresponding norms

$$\|\boldsymbol{u}\|_{\Omega_{\mathrm{c}}}^2 = \langle \boldsymbol{u} , \boldsymbol{u} \rangle_{\Omega_{\mathrm{c}}}, \qquad \|a\|_{\bar{\Omega}_{\mathrm{g}}}^2 = \langle a , a \rangle_{\bar{\Omega}_{\mathrm{g}}},$$

where $\sqrt{\mathring{g}_h} := \dfrac{2h_1 h_2}{h_1^2 + h_2^2} \sqrt{\mathring{g}_h}$ is the numerical Jacobian with respect to the default coordinate (ξ^1, ξ^2). Applying Proposition 1 in the skewed directions $\mathring{\xi}_1$ and $\mathring{\xi}_2$, it is easy to derive the following discrete identities:

LEMMA 3.1. *Let $\boldsymbol{u} \in L^2(\Omega_{\mathrm{c}}, \mathbb{R}^2)$ and $a \in L^2(\bar{\Omega}_{\mathrm{g}}, \mathbb{R})$. We have*
  1.

$$(3.39) \qquad\qquad\qquad \langle \boldsymbol{u} , \mathring{\nabla}_h a \rangle_{\Omega_{\mathrm{c}}} = -\langle \mathring{\nabla}'_h \cdot \boldsymbol{u} , a \rangle_{\bar{\Omega}_{\mathrm{g}}}$$
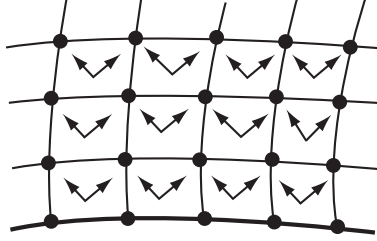
11

Fig. 3.4. *Positions of velocity field ($\searrow$ and $\nearrow$), vorticity and pressure ($\bullet$) for the generalized MAC scheme (3.44).*

2.

$$(3.40) \qquad \langle\, \boldsymbol{u}\,,\, \overset{\times}{\nabla}_h^{\perp} a\,\rangle_{\Omega_{\mathrm{c}}} = -\langle\, \overset{\times}{\nabla}_h^{\perp\prime}\cdot\boldsymbol{u}\,,\, a\,\rangle_{\bar{\Omega}_{\mathrm{g}}}$$

3.

$$(3.41) \qquad \overset{\times}{\nabla}_h' \cdot \overset{\times}{\nabla}_h a = \overset{\times}{\nabla}_h^{\perp\prime}\cdot\overset{\times}{\nabla}_h^{\perp} a = \overset{\times}{\triangle}_h' a \quad on\ \bar{\Omega}_{\mathrm{g}};$$

4. *If $a \in L^2(\bar{\Omega}_{\mathrm{g}}, \mathbb{R})$, then*

$$(3.42) \qquad \overset{\times}{\nabla}_h' \cdot \overset{\times}{\nabla}_h^{\perp} a = \overset{\times}{\nabla}_h^{\perp\prime}\cdot\overset{\times}{\nabla}_h a = 0 \quad on\ \overset{\circ}{\Omega}_{\mathrm{g}}.$$

In addition, if $a \in L_c^2(\bar{\Omega}_{\mathrm{g}}, \mathbb{R})$, then

$$(3.43) \qquad \overset{\times}{\nabla}_h' \cdot \overset{\times}{\nabla}_h^{\perp} a = \overset{\times}{\nabla}_h^{\perp\prime}\cdot\overset{\times}{\nabla}_h a = 0 \quad on\ \bar{\Omega}_{\mathrm{g}}.$$

3.3. Generalized MAC Scheme. On a curvilinear domain, we place both components of the velocity on cell centers $\boldsymbol{x}(\xi^1_{i+\frac{1}{2}}, \xi^2_{j+\frac{1}{2}})$, while the pressure and the vorticity are both placed on the grid points $\boldsymbol{x}(\xi^1_i, \xi^2_j)$ as shown in Figure 3.4.

The generalized MAC scheme with $\boldsymbol{u}$ defined on cell centers (GMACc) can be summarized as follows:

The GMACc Scheme:

Solve for $\boldsymbol{u} \in C^1([0, T]; L^2(\Omega_{\mathrm{c}}, \mathbb{R}^2))$ and $p \in C^0([0, T]; L^2(\bar{\Omega}_{\mathrm{g}}, \mathbb{R}))$ such that

$$(3.44) \qquad \begin{aligned} \boldsymbol{u}_t + \bar{\omega}\boldsymbol{u}^{\perp} + \overset{\times}{\nabla}_h p &= \nu\overset{\times}{\nabla}_h^{\perp}\omega + \boldsymbol{f} &\quad &\text{on } \Omega_{\mathrm{c}} \\ \omega &= \overset{\times}{\nabla}_h^{\perp\prime}\cdot\boldsymbol{u} &\quad &\text{on } \bar{\Omega}_{\mathrm{g}} \\ \overset{\times}{\nabla}_h'\cdot\boldsymbol{u} &= 0 &\quad &\text{on } \bar{\Omega}_{\mathrm{g}} \end{aligned}$$

where $\bar{\omega}_{i-\frac{1}{2}, j-\frac{1}{2}} = \frac{1}{4}(\omega_{i,j} + \omega_{i-1,j} + \omega_{i,j-1} + \omega_{i-1,j-1})$.

Another version of the generalized MAC scheme, GMACg, with $\boldsymbol{u}$ defined on grids and p on cell centers, is detailed in Appendix A.

As a direct consequence of (3.39-3.40), we have the following discrete energy estimate for (3.44):

LEMMA 3.2. *Let $(\boldsymbol{u}, p, \omega)$ be a solution to (3.44) with $\boldsymbol{f} = \boldsymbol{0}$, then*

$$\frac{1}{2}\frac{d}{dt}\|\boldsymbol{u}\|^2_{\Omega_{\mathrm{c}}} + \nu\|\omega\|^2_{\bar{\Omega}_{\mathrm{g}}} = 0.$$

It is worth noting that the reduced divergence operator in the third equation of (3.44) has implicitly incorporated the no-penetration condition $\boldsymbol{u}\cdot\boldsymbol{n} = 0$ in a natural way. On the other hand, the reduced curl operator in the second equation of (3.44) has implicitly incorporated the no-slip condition $\boldsymbol{u}\times\boldsymbol{n} = \boldsymbol{0}$ on Γ_{g}. This can be interpreted as a local vorticity boundary condition.

3.3.1. Non-homogeneous boundary velocity. In case of inhomogeneous boundary velocity $\boldsymbol{u} = \boldsymbol{u}_b$ on Γ, such as the driven cavity flow, the corresponding reduced operators requires proper modification.

Let $F \in L^2(\Omega_c, \mathbb{R})$ and $f \in L^2(\Gamma_c, \mathbb{R})$. With slight abuse of notations, we define the extended reduced operators, still denoted by $\overset{\times}{\mathring{D}}'_1$, $\overset{\times}{\mathring{D}}'_2$, as follows:

$$(3.45) \qquad \overset{\times}{\mathring{D}}'_1, \quad \overset{\times}{\mathring{D}}'_2 \quad : L^2(\Omega_c, \mathbb{R}) \times L^2(\Gamma_c, \mathbb{R}) \mapsto L^2(\bar{\Omega}_g, \mathbb{R}),$$

$$(3.46) \qquad \overset{\times}{\mathring{D}}'_1(F \oplus f)_{i,j} := \begin{cases} \dfrac{F_{i+\frac{1}{2},j+\frac{1}{2}} - F_{i-\frac{1}{2},j-\frac{1}{2}}}{\overset{\times}{h}} & \text{on } \mathring{\Omega}_g; \\[2ex] \dfrac{F_{i+\frac{1}{2},\frac{1}{2}} - \frac{1}{2}(f_{i+\frac{1}{2},0} + f_{i-\frac{1}{2},0})}{\frac{1}{2}\overset{\times}{h}} & 0 < i < M, \ j = 0; \\[2ex] \dfrac{F_{\frac{1}{2},\frac{1}{2}} - \frac{1}{2}(f_{0,\frac{1}{2}} + f_{\frac{1}{2},0})}{\frac{1}{4}\overset{\times}{h}} & (i,j) = (0,0). \end{cases}$$

$$(3.47) \qquad \overset{\times}{\mathring{D}}'_2(F \oplus f)_{i,j} := \begin{cases} \dfrac{F_{i-\frac{1}{2},j+\frac{1}{2}} - F_{i+\frac{1}{2},j-\frac{1}{2}}}{\overset{\times}{h}} & \text{on } \mathring{\Omega}_g; \\[2ex] \dfrac{F_{i-\frac{1}{2},\frac{1}{2}} - \frac{1}{2}(f_{i+\frac{1}{2},0} + f_{i-\frac{1}{2},0})}{\frac{1}{2}\overset{\times}{h}} & 0 < i < M, \ j = 0; \\[2ex] \dfrac{f_{0,\frac{1}{2}} - f_{\frac{1}{2},0}}{\frac{1}{2}\overset{\times}{h}} & (i,j) = (0,0). \end{cases}$$

One can define $\overset{\times}{\nabla}'_h \cdot$ and $\overset{\times}{\nabla}_h^{\perp\prime} \cdot : L^2(\Omega_c, \mathbb{R}^2) \times L^2(\Gamma_c, \mathbb{R}^2) \mapsto L^2(\bar{\Omega}_g, \mathbb{R})$ in a natural way.

When the boundary data is identically zero, (3.46)-(3.47) reduce to the original reduced operators,

$$(3.48) \qquad \overset{\times}{\mathring{D}}'_\alpha(F \oplus 0) = \overset{\times}{\mathring{D}}'_\alpha F.$$

$$(3.49) \qquad \overset{\times}{\nabla}'_h \cdot (\boldsymbol{u} \oplus \boldsymbol{0}) = \overset{\times}{\nabla}'_h \cdot \boldsymbol{u}, \quad \overset{\times}{\nabla}_h^{\perp\prime} \cdot (\boldsymbol{u} \oplus \boldsymbol{0}) = \overset{\times}{\nabla}_h^{\perp\prime} \cdot \boldsymbol{u}.$$

The corresponding scheme for inhomogeneous boundary velocity is given by

$$(3.50) \qquad \begin{aligned} \boldsymbol{u}_t + \bar{\omega}\boldsymbol{u}^\perp + \overset{\times}{\nabla}_h p &= \nu \overset{\times}{\nabla}_h^\perp \omega + \boldsymbol{f} & \text{on } \Omega_c \\ \omega &= \overset{\times}{\nabla}_h^{\perp\prime} \cdot (\boldsymbol{u} \oplus \boldsymbol{u}_b) & \text{on } \bar{\Omega}_g \\ \overset{\times}{\nabla}'_h \cdot (\boldsymbol{u} \oplus \boldsymbol{u}_b) &= 0 & \text{on } \bar{\Omega}_g \end{aligned}$$

subject to the following compatibility condition for the boundary velocity $\boldsymbol{u}_b$:

$$(3.51) \qquad \langle \, \boldsymbol{1}_{\bar{\Omega}_{g_e}} \, , \, \overset{\times}{\nabla}'_h \cdot (\boldsymbol{0} \oplus \boldsymbol{u}_b) \, \rangle_{\bar{\Omega}_g} = 0 = \langle \, \boldsymbol{1}_{\bar{\Omega}_{g_o}} \, , \, \overset{\times}{\nabla}'_h \cdot (\boldsymbol{0} \oplus \boldsymbol{u}_b) \, \rangle_{\bar{\Omega}_g}.$$

To see this, we first note that the kernel of $\overset{\times}{\nabla}_h$ consists of linear combinations of indicator functions of $\bar{\Omega}_{g_e}$ and $\bar{\Omega}_{g_o}$:

$$(3.52) \qquad \ker(\overset{\times}{\nabla}_h) = \text{span}\{\boldsymbol{1}_{\bar{\Omega}_{g_e}}, \boldsymbol{1}_{\bar{\Omega}_{g_o}}\}.$$

From (3.48), (3.39) and (3.52), it follows that for all c_1, $c_2 \in \mathbb{R}$,

(3.53)
$$\langle c_1 \mathbf{1}_{\bar{\Omega}_{\mathrm{ge}}} + c_2 \mathbf{1}_{\bar{\Omega}_{\mathrm{go}}} , \overset{\times}{\nabla}'_h \cdot (\boldsymbol{u} \oplus \boldsymbol{u}_b) \rangle_{\bar{\Omega}_{\mathrm{g}}} = \langle c_1 \mathbf{1}_{\bar{\Omega}_{\mathrm{ge}}} + c_2 \mathbf{1}_{\bar{\Omega}_{\mathrm{go}}} , \overset{\times}{\nabla}'_h \cdot (\boldsymbol{u} \oplus \boldsymbol{0}) + \overset{\times}{\nabla}'_h \cdot (\boldsymbol{0} \oplus \boldsymbol{u}_b) \rangle_{\bar{\Omega}_{\mathrm{g}}}$$
$$= \langle c_1 \mathbf{1}_{\bar{\Omega}_{\mathrm{ge}}} + c_2 \mathbf{1}_{\bar{\Omega}_{\mathrm{go}}} , \overset{\times}{\nabla}'_h \cdot (\boldsymbol{0} \oplus \boldsymbol{u}_b) \rangle_{\bar{\Omega}_{\mathrm{g}}}$$

In view of (3.53) and the 3rd equation of (3.50), the compatibility condition (3.51) follows. It is easy to see that both conditions in (3.51) can be interpreted naturally as discrete analogue of $\int_{\Gamma} \boldsymbol{u}_b \cdot \boldsymbol{n} = 0$ since

$$\langle \mathbf{1}_{\bar{\Omega}_{\mathrm{ge}}} , \overset{\times}{\nabla}'_h \cdot (\boldsymbol{0} \oplus \boldsymbol{u}_b) \rangle_{\bar{\Omega}_{\mathrm{g}}} = \langle \mathbf{1}_{\bar{\Omega}_{\mathrm{go}}} , \overset{\times}{\nabla}'_h \cdot (\boldsymbol{0} \oplus \boldsymbol{u}_b) \rangle_{\bar{\Omega}_{\mathrm{g}}} = \frac{1}{2} \sum_{\Gamma_{\mathrm{c}}} \boldsymbol{u}_b \cdot \boldsymbol{n} \, \Delta \ell_h$$

(3.54)
$$= \frac{1}{2} \left(\sum_{i=1}^{M} \left((\boldsymbol{u}_b \cdot \boldsymbol{n} \, \Delta \ell_h)_{i-\frac{1}{2},0} + (\boldsymbol{u}_b \cdot \boldsymbol{n} \, \Delta \ell_h)_{i-\frac{1}{2},N} \right) + \sum_{j=1}^{N} \left((\boldsymbol{u}_b \cdot \boldsymbol{n} \, \Delta \ell_h)_{0,j-\frac{1}{2}} + (\boldsymbol{u}_b \cdot \boldsymbol{n} \, \Delta \ell_h)_{M,j-\frac{1}{2}} \right) \right)$$

where, for example

(3.55) $(\boldsymbol{u}_b \cdot \boldsymbol{n} \, \Delta \ell_h)_{i-\frac{1}{2},0} = \dfrac{h_1 h_2}{\overset{\times}{h}} \left(\sqrt{g_h}(-\overset{\times}{u}_b^2 - \overset{\times}{u}_b^1) \right)_{i-\frac{1}{2},0} , \quad (\boldsymbol{u}_b \cdot \boldsymbol{n} \, \Delta \ell_h)_{0,j-\frac{1}{2}} = \dfrac{h_1 h_2}{\overset{\times}{h}} \left(\sqrt{g_h}(\overset{\times}{u}_b^2 - \overset{\times}{u}_b^1) \right)_{0,j-\frac{1}{2}} ,$

with

(3.56)
$$(\boldsymbol{u}_b \cdot \boldsymbol{n})_{i-\frac{1}{2},0} = \left(\frac{-u_b^2}{\sqrt{g^{22}}} \right)_{i-\frac{1}{2},0} = \left(\frac{(-\overset{\times}{u}_b^2 - \overset{\times}{u}_b^1)h_2}{\overset{\times}{h}\sqrt{g^{22}}} \right)_{i-\frac{1}{2},0}$$
$$(\boldsymbol{u}_b \cdot \boldsymbol{n})_{0,j-\frac{1}{2}} = \left(\frac{-u_b^1}{\sqrt{g^{11}}} \right)_{0,j-\frac{1}{2}} = \left(\frac{(\overset{\times}{u}_b^2 - \overset{\times}{u}_b^1)h_1}{\overset{\times}{h}\sqrt{g^{11}}} \right)_{0,j-\frac{1}{2}}$$

(3.57)
$$(\Delta \ell_h)_{i-\frac{1}{2},0} := (h_1 \sqrt{g_h} \sqrt{g^{22}})_{i-\frac{1}{2},0} = (h_1 \frac{\sqrt{g_h}}{\sqrt{g}} \sqrt{g_{11}})_{i-\frac{1}{2},0} \approx \Delta \xi^1 \left| \frac{\partial \boldsymbol{x}}{\partial \xi^1} \right|_{i-\frac{1}{2},0}$$
$$(\Delta \ell_h)_{0,j-\frac{1}{2}} := (h_2 \sqrt{g_h} \sqrt{g^{11}})_{0,j-\frac{1}{2}} = (h_2 \frac{\sqrt{g_h}}{\sqrt{g}} \sqrt{g_{22}})_{0,j-\frac{1}{2}} \approx \Delta \xi^2 \left| \frac{\partial \boldsymbol{x}}{\partial \xi^2} \right|_{0,j-\frac{1}{2}}$$

and similarly on $(i - \frac{1}{2}, N)$ and $(M, j - \frac{1}{2})$.

REMARK 1. In case of complex geometry, it may be necessary to patch the domain with several non-overlapping coordinate charts as illustrated in Figure 4.1. In this case, the metric tensor has a jump discontinuity across coordinate boundaries. We define the discrete divergence operator at a grid point P on the coordinate interface by

(3.58)
$$(\overset{\times}{\nabla}_h \cdot \boldsymbol{u})_P = \frac{\left(\frac{1}{2}\sqrt{\overset{\times}{g}_h} \overset{\times}{\nabla}'_h \cdot \boldsymbol{u} \right)_{P_{(+)}} + \left(\frac{1}{2}\sqrt{\overset{\times}{g}_h} \overset{\times}{\nabla}'_h \cdot \boldsymbol{u} \right)_{P_{(-)}}}{\left(\sqrt{\overset{\times}{g}_h} \right)_{P_{(+)}} + \left(\sqrt{\overset{\times}{g}_h} \right)_{P_{(-)}}}$$

At a multiple coordinate junction Q, such as the one given in Figure 3.5, the formula becomes

(3.59)
$$(\overset{\times}{\nabla}_h \cdot \boldsymbol{u})_Q = \left(\sum_{Q \in i\text{th chart}} \left(\sqrt{\overset{\times}{g}_h} \right)_{Q_{(i)}} \right)^{-1} \sum_{Q \in i\text{th chart}} \left(\frac{1}{4}\sqrt{\overset{\times}{g}_h} \overset{\times}{\nabla}'_h \cdot \boldsymbol{u} \right)_{Q_{(i)}}$$

A similar formula applies to discrete curl and discrete Laplacian. In this way, it is easy to see that the summation by parts identities in Lemma 3.1 remains valid. The same treatment for discrete Laplacian on material interface has been proposed for elliptic interface problems in [Wa, HWa].
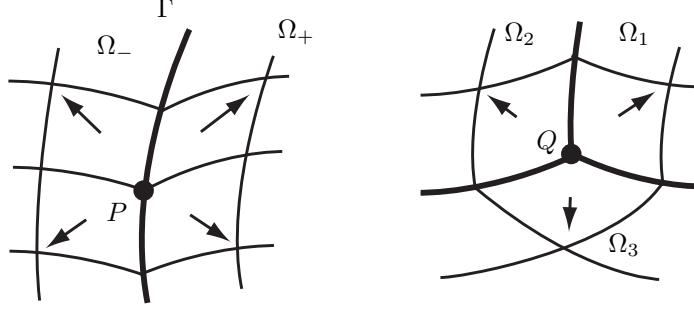
14

FIG. 3.5. *Schematic illustration of the discrete divergence at a point P on the coordinate interface Γ (left) and a triple coordinate junction Q (right).*

3.4. Explicit and Implicit Time Stepping.

3.4.1. Explicit Time Stepping and Hodge Decomposition. As in section 2, we illustrate the time stepping by the forward Euler method:

$$
(3.60) \quad
\begin{aligned}
\frac{\boldsymbol{u}^{n+1} - \boldsymbol{u}^n}{\Delta t} + (\bar{\omega}\boldsymbol{u}^{\perp})^n + \overset{\times}{\nabla}_h p^{n+1} &= \nu \overset{\times}{\nabla}_h^{\perp} \omega^n + \boldsymbol{f}^n && \text{on } \Omega_{\text{c}} \\
\omega^n &= \overset{\times}{\nabla}_h^{\perp \prime} \cdot (\boldsymbol{u}^n \oplus \boldsymbol{u}_b^n) && \text{on } \bar{\Omega}_{\text{g}} \\
\overset{\times}{\nabla}_h' \cdot (\boldsymbol{u}^{n+1} \oplus \boldsymbol{u}_b^{n+1}) &= 0 && \text{on } \bar{\Omega}_{\text{g}}
\end{aligned}
$$

In high Reynolds number calculations, a high order Runge-Kutta method such as RK4 is needed for stability consideration [EL].

Given $(\boldsymbol{u}^n, p^n)$ with $\overset{\times}{\nabla}_h' \cdot (\boldsymbol{u}^n \oplus \boldsymbol{u}_b^n) = 0$, (3.60) is solved via the following steps:
Step 1. Evaluate ω^n up to the boundary

$$
(3.61) \qquad \omega^n = \overset{\times}{\nabla}_h^{\perp \prime} \cdot (\boldsymbol{u}^n \oplus \boldsymbol{u}_b^n) \qquad \text{on } \bar{\Omega}_{\text{g}}.
$$

Step 2. Evaluate $\boldsymbol{u}^*$ on cell centers

$$
(3.62) \qquad \frac{\boldsymbol{u}^* - \boldsymbol{u}^n}{\Delta t} + (\bar{\omega}\boldsymbol{u}^{\perp})^n = \nu \overset{\times}{\nabla}_h^{\perp} \omega^n + \boldsymbol{f}^n \qquad \text{on } \Omega_{\text{c}}.
$$

Step 3. Solve for $(\boldsymbol{u}^{n+1}, p^{n+1})$ such that

$$
(3.63) \qquad
\begin{aligned}
\frac{\boldsymbol{u}^{n+1} - \boldsymbol{u}^*}{\Delta t} + \overset{\times}{\nabla}_h p^{n+1} &= \boldsymbol{0} && \text{on } \Omega_{\text{c}}, \\
\overset{\times}{\nabla}_h' \cdot (\boldsymbol{u}^{n+1} \oplus \boldsymbol{u}_b^{n+1}) &= 0 && \text{on } \bar{\Omega}_{\text{g}},
\end{aligned}
$$

This is the (inhomogeneous) Hodge decomposition for $\boldsymbol{u}^*$ and can be performed as follows:
Step 3-1. Solve for p^{n+1} up to the boundary from

$$
(3.64) \qquad \overset{\times}{\triangle}_h' p^{n+1} = \frac{1}{\Delta t} \overset{\times}{\nabla}_h' \cdot (\boldsymbol{u}^* \oplus \boldsymbol{u}_b^{n+1}) \qquad \text{on } \bar{\Omega}_{\text{g}}.
$$

15

Step 3-2. Update $\boldsymbol{u}^{n+1}$ from

$$(3.65) \qquad \frac{\boldsymbol{u}^{n+1} - \boldsymbol{u}^*}{\Delta t} + \overset{\times}{\nabla}_h p^{n+1} = \boldsymbol{0} \qquad \text{on } \Omega_{\mathrm{c}}.$$

It follows from (3.41, 3.49, 3.64, 3.65) that

$$
\begin{aligned}
\overset{\times}{\nabla}'_h \cdot (\boldsymbol{u}^{n+1} \oplus \boldsymbol{u}_b^{n+1}) &= \overset{\times}{\nabla}'_h \cdot (\boldsymbol{u}^* \oplus \boldsymbol{u}_b^{n+1}) + \overset{\times}{\nabla}'_h \cdot \big((\boldsymbol{u}^{n+1} - \boldsymbol{u}^*) \oplus \boldsymbol{0}\big) \\
&= \overset{\times}{\nabla}'_h \cdot (\boldsymbol{u}^* \oplus \boldsymbol{u}_b^{n+1}) + \overset{\times}{\nabla}'_h \cdot (\boldsymbol{u}^{n+1} - \boldsymbol{u}^*) \\
&= 0.
\end{aligned}
$$

Step 1 can be viewed as a vorticity boundary condition that incorporates the tangential component of $\boldsymbol{u}_b$. On the other hand, step 3 depends on $\boldsymbol{u}_b$ only through its normal component. In step 3-1, the pressure is solved as a Lagrangian multiplier without introducing the ghost value and artificial pressure boundary conditions. From (3.39) and (3.41), it is easy to see that

$$(3.66) \qquad \langle q\,,\, \overset{\times}{\triangle}'_h p \rangle_{\bar{\Omega}_{\mathrm{g}}} = -\langle \overset{\times}{\nabla}_h q\,,\, \overset{\times}{\nabla}_h p \rangle_{\Omega_{\mathrm{c}}} = -h_1 h_2 \sum_{i=1}^{M} \sum_{j=1}^{N} \Big(\sqrt{g_h} \sum_{\mu,\nu=1,2} \overset{\times}{g}_h^{\mu\nu}(\overset{\times}{D}_\mu p)(\overset{\times}{D}_\nu q)\Big)_{i-\frac{1}{2},j-\frac{1}{2}}.$$

In other words, $\overset{\times}{\triangle}'_h$ is self-adjoint with respect to the inner product (3.38) and non-positive definite as long as each of the 2×2 matrices $\big(\{\overset{\times}{g}_h^{\mu\nu}\}_{\mu,\nu=1}^2\big)_{i-\frac{1}{2},j-\frac{1}{2}}$ is positive definite on the cell centers. This only requires the cells to be non-singular. No further grid regularity is needed for stability concerns. In addition,

$$(3.67) \qquad \ker(\overset{\times}{\triangle}'_h) = \ker(\overset{\times}{\nabla}_h) = \mathrm{span}\{\boldsymbol{1}_{\bar{\Omega}_{\mathrm{g_e}}}, \boldsymbol{1}_{\bar{\Omega}_{\mathrm{g_o}}}\}$$

thus (3.64) is solvable if and only if

$$(3.68) \qquad \langle c_1 \boldsymbol{1}_{\bar{\Omega}_{\mathrm{g_e}}} + c_2 \boldsymbol{1}_{\bar{\Omega}_{\mathrm{g_o}}}\,,\, \overset{\times}{\nabla}'_h \cdot (\boldsymbol{u}^* \oplus \boldsymbol{u}_b^n) \rangle_{\bar{\Omega}_{\mathrm{g}}} = 0 \qquad \text{for all } c_1, c_2 \in R.$$

In view of (3.53), it follows that the solvability condition for (3.64) is exactly the compatibility condition (3.51). In addition, it is worth noting that (3.64) can be decoupled and solved on $\bar{\Omega}_{\mathrm{g_e}}$ and $\bar{\Omega}_{\mathrm{g_o}}$ separately.

3.4.2. Implicit Time Stepping and Nonlinear Stability. Here we list a few partially and fully implicit 2nd order time discretizations of our scheme.

For low Reynolds number flows, explicit time stepping is subject to parabolic time stepping constraint [EL]. As an alternative, the Stokes-based partially implicit time stepping is given by:

$$
(3.69) \qquad
\begin{aligned}
\frac{\boldsymbol{u}^{n+1} - \boldsymbol{u}^n}{2\Delta t} + N_h(\boldsymbol{u}^{n+\frac{1}{2}}) + \frac{1}{2}(\overset{\times}{\nabla}_h p^{n+1} + \overset{\times}{\nabla}_h p^n) &= \frac{1}{2}\nu(\overset{\times}{\nabla}^{\perp}_h \omega^{n+1} + \overset{\times}{\nabla}^{\perp}_h \omega^n) + \boldsymbol{f}^{n+\frac{1}{2}} & \text{on } \Omega_{\mathrm{c}} \\
\omega^{n+1} &= \overset{\times}{\nabla}^{\perp\prime}_h \cdot (\boldsymbol{u}^{n+1} \oplus \boldsymbol{u}_b^{n+1}) & \text{on } \bar{\Omega}_{\mathrm{g}} \\
\overset{\times}{\nabla}'_h \cdot (\boldsymbol{u}^{n+1} \oplus \boldsymbol{u}_b^{n+1}) &= 0 & \text{on } \bar{\Omega}_{\mathrm{g}}
\end{aligned}
$$

where $N_h(\boldsymbol{u}^{n+\frac{1}{2}}) = \frac{3}{2}\bar{\omega}^n(\boldsymbol{u}^n)^\perp - \frac{1}{2}\bar{\omega}^{n-1}(\boldsymbol{u}^{n-1})^\perp$.

It is not clear what the time stepping constraint for (3.69) is. Alternatively, one can discretize the nonlinear term semi-implicitly or fully implicitly to allow larger time steps. The special structure of our discretization of the nonlinear term guarantees unconditional stability with second order backward difference time stepping (assuming $\boldsymbol{f} = \boldsymbol{0}$ and $\boldsymbol{u}_b = \boldsymbol{0}$):

$$
(3.70) \qquad
\begin{aligned}
\frac{3\boldsymbol{u}^{n+1} - 4\boldsymbol{u}^n + \boldsymbol{u}^{n-1}}{2\Delta t} + N_h(\boldsymbol{u}^{n+1}) + \overset{\times}{\nabla}_h p^{n+1} &= \nu\overset{\times}{\nabla}^{\perp}_h \omega^{n+1} & \text{on } \Omega_{\mathrm{c}} \\
\omega^{n+1} &= \overset{\times}{\nabla}^{\perp\prime}_h \cdot \boldsymbol{u}^{n+1} & \text{on } \bar{\Omega}_{\mathrm{g}} \\
\overset{\times}{\nabla}'_h \cdot \boldsymbol{u}^{n+1} &= 0 & \text{on } \bar{\Omega}_{\mathrm{g}}
\end{aligned}
$$

16

where $N_h(\boldsymbol{u}^{n+1}) = (2\bar{\omega}^n - \bar{\omega}^{n-1})(\boldsymbol{u}^{n+1})^\perp$ for semi-implicit scheme, or $N_h(\boldsymbol{u}^{n+1}) = \bar{\omega}^{n+1}(\boldsymbol{u}^{n+1})^\perp$ for fully implicit scheme.

To see the stability of (3.70), we take the inner product of (3.70) with $\boldsymbol{u}^{n+1}$ to get

$$\langle\, \boldsymbol{u}^{n+1}\,,\, \frac{3\boldsymbol{u}^{n+1} - 4\boldsymbol{u}^n + \boldsymbol{u}^{n-1}}{2\Delta t}\,\rangle_{\Omega_c} + \nu\|\omega^{n+1}\|_{\bar{\Omega}_g}^2 = 0.$$

This gives

$$\frac{3\|\boldsymbol{u}^{n+1}\|_{\Omega_c}^2 - 4\|\boldsymbol{u}^n\|_{\Omega_c}^2 + \|\boldsymbol{u}^{n-1}\|_{\Omega_c}^2}{4\Delta t} + \frac{4\|\boldsymbol{u}^{n+1} - \boldsymbol{u}^n\|_{\Omega_c}^2 - \|\boldsymbol{u}^{n+1} - \boldsymbol{u}^{n-1}\|_{\Omega_c}^2}{4\Delta t} + \nu\|\omega^{n+1}\|_{\bar{\Omega}_g}^2 = 0.$$

With the inequality $\|\boldsymbol{u}^{n+1} - \boldsymbol{u}^{n-1}\|_{\Omega_c}^2 \leq 2(\|\boldsymbol{u}^{n+1} - \boldsymbol{u}^n\|_{\Omega_c}^2 + \|\boldsymbol{u}^n - \boldsymbol{u}^{n-1}\|_{\Omega_c}^2)$, one obtains

$$3\|\boldsymbol{u}^{n+1}\|_{\Omega_c}^2 - \|\boldsymbol{u}^n\|_{\Omega_c}^2 - 3\|\boldsymbol{u}^1\|_{\Omega_c}^2 + \|\boldsymbol{u}^0\|_{\Omega_c}^2 + 2\|\boldsymbol{u}^{n+1} - \boldsymbol{u}^n\|_{\Omega_c}^2 - 2\|\boldsymbol{u}^1 - \boldsymbol{u}^0\|_{\Omega_c}^2 + 4\nu\Delta t\sum_{k=2}^{n+1}\|\omega^k\|_{\bar{\Omega}_g}^2 \leq 0,$$

or

(3.71) $$\|\boldsymbol{u}^{n+1}\|_{\Omega_c}^2 + \|2\boldsymbol{u}^{n+1} - \boldsymbol{u}^n\|_{\Omega_c}^2 + 4\nu\Delta t\sum_{k=2}^{n+1}\|\omega^k\|_{\bar{\Omega}_g}^2 \leq 3\|\boldsymbol{u}^1\|_{\Omega_c}^2 + 2\|\boldsymbol{u}^1 - \boldsymbol{u}^0\|_{\Omega_c}^2 - \|\boldsymbol{u}^0\|_{\Omega_c}^2.$$

This gives unconditionally stability of (3.70).

Similarly, for steady state calculations with pseudo-time stepping where Δt may vary spatially, it is not difficult to see that the 1st order BDF formula

(3.72)
$$\begin{aligned}
\frac{\boldsymbol{u}^{n+1} - \boldsymbol{u}^n}{\Delta t} + N_h(\boldsymbol{u}^{n+1}) + \overset{\times}{\nabla}_h p^{n+1} &= \nu\overset{\times}{\nabla}_h^\perp \omega^{n+1} &\text{on } \Omega_c \\
\omega^{n+1} &= \overset{\times}{\nabla}_h^{\perp\prime} \cdot \boldsymbol{u}^{n+1} &\text{on } \bar{\Omega}_g \\
\overset{\times}{\nabla}_h^\prime \cdot \boldsymbol{u}^{n+1} &= 0 &\text{on } \bar{\Omega}_g
\end{aligned}$$

with $N_h(\boldsymbol{u}^{n+1}) = \bar{\omega}^n(\boldsymbol{u}^{n+1})^\perp$ or $N_h(\boldsymbol{u}^{n+1}) = \bar{\omega}^{n+1}(\boldsymbol{u}^{n+1})^\perp$ also leads to unconditional stability:

(3.73) $$\frac{1}{2}\|\frac{\boldsymbol{u}^n}{\sqrt{\Delta t}}\|_{\Omega_c}^2 + \frac{1}{2}\sum_{k=1}^n\|\frac{\boldsymbol{u}^k - \boldsymbol{u}^{k-1}}{\sqrt{\Delta t}}\|_{\Omega_c}^2 + \nu\sum_{k=1}^n\|\omega^k\|_{\bar{\Omega}_g}^2 \leq \frac{1}{2}\|\frac{\boldsymbol{u}^0}{\sqrt{\Delta t}}\|_{\Omega_c}^2.$$

3.5. Comparison with Similarly Staggered Schemes. It can be shown that GMAC is second order accurate on smooth grids in 2D for both velocity and pressure [HLW]. A key ingredient in the pressure error estimate for (3.44) is the inf-sup (LBB) condition which states that there exists a constant β, independent of the grid size, such that

(3.74) $$\inf_{p\in L^2(\bar{\Omega}_g,\mathbb{R})/\mathbb{R}^2}\sup_{\boldsymbol{u}\in L^2(\Omega_c,\mathbb{R}^2)} \frac{\langle\, p\,,\, \overset{\times}{\nabla}_h^\prime \cdot \boldsymbol{u}\,\rangle_{\bar{\Omega}_g}}{\|p\|_{\bar{\Omega}_g}\big(\|\boldsymbol{u}\|_{\Omega_c}^2 + \|\overset{\times}{\nabla}_h^{\perp\prime} \cdot \boldsymbol{u}\|_{\bar{\Omega}_g}^2 + \|\overset{\times}{\nabla}_h^\prime \cdot \boldsymbol{u}\|_{\bar{\Omega}_g}^2\big)^{\frac{1}{2}}} := \beta_h \geq \beta$$

Roughly speaking, the higher the ratio $\text{DOF}(\boldsymbol{u})/\text{DOF}(p)$ is, the more likely the inf-sup condition (3.74) is to hold true and be verified.

On 2D quadrilateral meshes, some numerical schemes are known to satisfy the inf-sup condition (3.74), including the $Q_\ell - P_{\ell-1}$ elements, $\ell \geq 2$ [GR] with $\text{DOF}(\boldsymbol{u})/\text{DOF}(p)\geq 8/3$, the $\mathscr{Q}_1 - P_0$ element [GR] with $\text{DOF}(\boldsymbol{u})/\text{DOF}(p)= 3$, and the schemes proposed in [Cho], [Han] and [RaTu] with $\text{DOF}(\boldsymbol{u})/\text{DOF}(p) \geq 4$. Here $\text{DOF}(\boldsymbol{u})$ is the degree of freedom for the velocity field, counting both components.
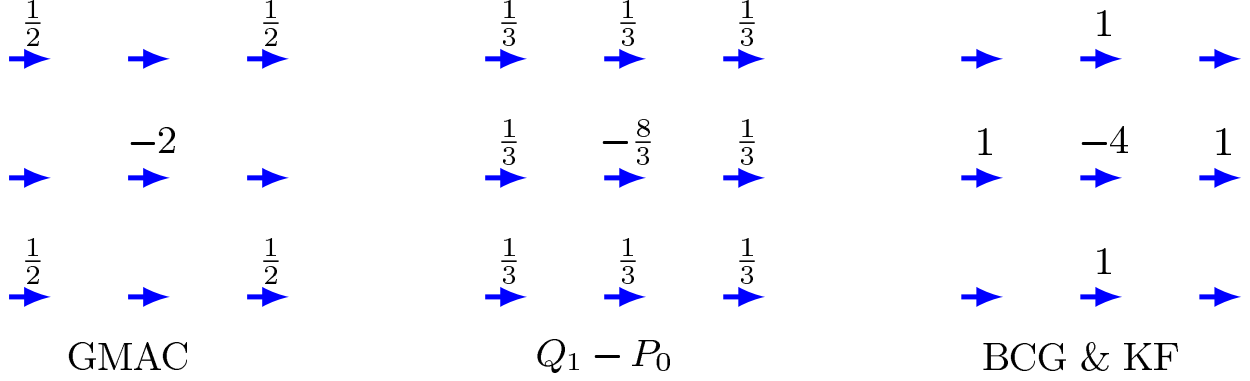
FIG. 3.6. *Comparison of vector Laplacian for various schemes*

When the ratio of degrees of freedom becomes marginal, the compatibility of spatial discretization plays the key role in establishing the inf-sup condition. This is the case for the classical MAC scheme [HW] and GMAC scheme.

To demonstrate this point more clearly, we compare GMAC ((3.44) and (A.17)) against similarly staggered schemes with different (and non-compatible) spatial discretizations, including the BCG scheme (Bell, Colella and Glaz [BCG]), the KF scheme (Kuznetsov, Fortin et al [FPT, Ku, PT]), and the $Q_1 - P_0$ element. For simplicity of presentation, all the discretization formula throughout this subsection refer to interior nodes only. Proper reductions are required on the boundary for all these schemes. We omit the details.

Recall the spatial discretization of the classical MAC scheme on 2D uniform Cartesian grids are given by
(3.75)
$$\triangle_h u_{i,j-\frac{1}{2}} = \frac{1}{h^2}(u_{i+1,j-\frac{1}{2}} + u_{i-1,j-\frac{1}{2}} + u_{i,j+\frac{1}{2}} + u_{i,j-\frac{3}{2}} - 4u_{i,j-\frac{1}{2}}), \quad D_x p_{i,j-\frac{1}{2}} = \frac{1}{h}(p_{i+\frac{1}{2},j-\frac{1}{2}} - p_{i-\frac{1}{2},j-\frac{1}{2}})$$
$$\triangle_h v_{i-\frac{1}{2},j} = \frac{1}{h^2}(v_{i-\frac{1}{2},j+1} + v_{i-\frac{1}{2},j-1} + v_{i+\frac{1}{2},j} + v_{i-\frac{3}{2},j} - 4v_{i-\frac{1}{2},j}), \quad D_y p_{i-\frac{1}{2},j} = \frac{1}{h}(p_{i-\frac{1}{2},j+\frac{1}{2}} - p_{i-\frac{1}{2},j-\frac{1}{2}})$$

Like the MAC scheme, the discretization of the viscous term for BCG, KF use standard five point formula. Take the KF scheme for example,

(3.76)
$$\triangle_h u_{i,j} = \frac{1}{h^2}(u_{i+1,j} + u_{i-1,j} + u_{i,j+1} + u_{i,j-1} - 4u_{i,j}),$$
$$\triangle_h v_{i,j} = \frac{1}{h^2}(v_{i+1,j} + v_{i-1,j} + v_{i,j+1} + v_{i,j-1} - 4u_{i,j}).$$

On the other hand, the pressure gradient for KF takes standard centered differencing, averaged in the transversal direction in order to maintain second order local truncation error,

(3.77)
$$(D_x p)_{i,j} = \frac{1}{2h}\left((p_{i+\frac{1}{2},j+\frac{1}{2}} - p_{i-\frac{1}{2},j+\frac{1}{2}}) + (p_{i+\frac{1}{2},j-\frac{1}{2}} - p_{i-\frac{1}{2},j-\frac{1}{2}})\right),$$
$$(D_y p)_{i,j} = \frac{1}{2h}\left((p_{i+\frac{1}{2},j+\frac{1}{2}} - p_{i+\frac{1}{2},j-\frac{1}{2}}) + (p_{i-\frac{1}{2},j+\frac{1}{2}} - p_{i-\frac{1}{2},j-\frac{1}{2}})\right).$$

Similar averaging is also needed for the divergence free constraint.

In contrast, the viscous term in GMACc and GMACg are based on the skewed Laplacian. For example,

18

in GMACg we have

$$
\overset{\times}{\triangle}_h u_{i,j} = \frac{1}{2h^2}(u_{i+1,j+1} + u_{i-1,j+1} + u_{i+1,j-1} + u_{i-1,j+1} - 4u_{i,j})
$$

(3.78)

$$
\overset{\times}{\triangle}_h v_{i,j} = \frac{1}{2h^2}(v_{i+1,j+1} + v_{i-1,j+1} + v_{i+1,j-1} + v_{i-1,j+1} - 4v_{i,j}),
$$

and the same pressure gradient (3.77) as KF. Here we have adopted conventional vector notation in terms of the components u, v in the default coordinate $(\xi^1, \xi^2) = (x, y)$. That is, we write $\boldsymbol{u} = (u, v)$ if $\boldsymbol{u} = u\boldsymbol{e_x} + v\boldsymbol{e_y}$.

The well known div-unstable $Q_1 - P_0$ element corresponds to a mixture of standard and skewed Laplacian:

(3.79)
$$
\overset{*}{\triangle}_h = \frac{1}{3}\triangle_h + \frac{2}{3}\overset{\times}{\triangle}_h.
$$

and the same pressure gradient (3.77) as KF and GMACc.

The BCG and GMACc are identical to KF and GMACg respectively except for the half-grid shift in the placement of variables. We can summarize these discretizations as follows

(3.80)
$$
\nabla^2_{\mathrm{BCG}} \boldsymbol{u}_{i+\frac{1}{2},j+\frac{1}{2}} = \left(\triangle_h u_{i+\frac{1}{2},j+\frac{1}{2}}, \triangle_h v_{i+\frac{1}{2},j+\frac{1}{2}}\right),
$$

(3.81)
$$
\nabla^2_{\mathrm{GMACc}} \boldsymbol{u}_{i+\frac{1}{2},j+\frac{1}{2}} = \left(\overset{\times}{\triangle}_h u_{i+\frac{1}{2},j+\frac{1}{2}}, \overset{\times}{\triangle}_h v_{i+\frac{1}{2},j+\frac{1}{2}}\right),
$$

(3.82)
$$
\nabla^2_{\mathrm{KF}} \boldsymbol{u}_{i,j} = \left(\triangle_h u_{i,j}, \triangle_h v_{i,j}\right),
$$

(3.83)
$$
\nabla^2_{\mathrm{GMACg}} \boldsymbol{u}_{i,j} = \left(\overset{\times}{\triangle}_h u_{i,j}, \overset{\times}{\triangle}_h v_{i,j}\right),
$$

(3.84)
$$
\nabla^2_{Q_1 - P_0} \boldsymbol{u}_{i,j} = \left(\overset{*}{\triangle}_h u_{i,j}, \overset{*}{\triangle}_h v_{i,j}\right).
$$

Note that, in GMACc (3.44) and GMACg (A.17), the viscous term was originally proposed as $\overset{\times}{\nabla}{}^{\perp}_h \omega = \overset{\times}{\nabla}{}^{\perp}_h(\overset{\times}{\nabla}{}^{\perp}_h \cdot \boldsymbol{u})$, while in (3.81) and (3.83), it is recast in terms of the full vector Laplacian

(3.85)
$$
\nabla^2_{\mathrm{GMAC}} \boldsymbol{u} = \overset{\times}{\nabla}{}^2_h \boldsymbol{u} := \overset{\times}{\nabla}_h(\overset{\times}{\nabla}_h \cdot \boldsymbol{u}) + \overset{\times}{\nabla}{}^{\perp}_h(\overset{\times}{\nabla}{}^{\perp}_h \cdot \boldsymbol{u})
$$

to make the comparison more comprehensible.

Equation (3.85) is the 2D discrete analogue of the identity

(3.86)
$$
\nabla^2 \boldsymbol{u} = \nabla(\nabla \cdot \boldsymbol{u}) - \nabla \times \nabla \times \boldsymbol{u},
$$

and is algebraically identical to $\overset{\times}{\nabla}{}^{\perp}_h(\overset{\times}{\nabla}{}^{\perp}_h \cdot \boldsymbol{u})$ under the incompressibility constraint $\overset{\times}{\nabla}_h \cdot \boldsymbol{u} = 0$.

All these schemes are semi-staggered with $\mathrm{DOF}(\boldsymbol{u})/\mathrm{DOF}(p) = 2$ in 2D (lowest among discretizations based on quadrilateral meshes). They result in identical discretizations for the pressure gradient and incompressibility constraint, namely the skewed gradient $\overset{\times}{\nabla}_h$ and skewed divergence $\overset{\times}{\nabla}_h\cdot$. We believe that the spatial compatibility among the discrete gradient, divergence and curl (as part of the vector Laplacian) operators

(3.87)
$$
\overset{\times}{\nabla}{}^{\perp}_h \cdot \overset{\times}{\nabla}_h = \overset{\times}{\nabla}_h \cdot \overset{\times}{\nabla}{}^{\perp}_h = 0
$$

plays an important role in the uniform LBB estimate for GMAC. We will demonstrate this result by numerically computing the LBB constant in section 4. A rigorous proof of the inf-sup condition (3.74) for GMAC can be found in [HLW]. We remark here that the classical MAC scheme is fully staggered with $\mathrm{DOF}(\boldsymbol{u})/\mathrm{DOF}(p) = 2$ in 2D. It is shown in [HWu] that the classical MAC scheme with a different boundary condition also satisfies the inf-sup condition.

4. Numerical Result. In this section, we report several numerical test results. We start with the numerical computation of the LBB constants for the schemes mentioned in section 3.5. The result gives very strong indication on uniform LBB estimate for GMAC. We then proceed with standard convergence test and benchmark problems. We have observed clean second order accuracy in both velocity and pressure in the convergence test. The benchmark simulation also shows good agreement with the results reported in the literature.

Example 1: The LBB Constant β_h

It is well known [RaTu, BF] that the LBB constant can be obtained through a generalized singular value decomposition. Take GMACc for example, denote the matrix representations of the operators in (3.74) by

$$\mathbb{A} \sim \sqrt{\overset{\times}{g}}_{h,\mathrm{c}}\big(1 - \overset{\times}{\nabla}_h^{\perp}\overset{\times}{\nabla}_h^{\perp\prime}\cdot - \overset{\times}{\nabla}_h\overset{\times}{\nabla}_h^{\prime}\cdot\big), \quad \mathbb{B} \sim \sqrt{\overset{\times}{g}}_{h,\mathrm{g}}^{\prime}\overset{\times}{\nabla}_h^{\prime}\cdot, \quad \mathbb{B}^{\mathrm{T}} \sim -\sqrt{\overset{\times}{g}}_{h,\mathrm{c}}\overset{\times}{\nabla}_h, \quad \mathbb{M} \sim \sqrt{\overset{\times}{g}}_{h,\mathrm{g}}^{\prime},$$

where the $\sqrt{\overset{\times}{g}}_{h,\mathrm{c}}$ in $\mathbb{B}$ is defined on cell centers and $\sqrt{\overset{\times}{g}}_{h,\mathrm{g}}^{\prime}$ defined on grid points with standard weighting ($\frac{1}{2}$ on the edges and $\frac{1}{4}$ on corners). The LBB constant in (3.74) can be characterized as

(4.1)

$$\beta_h = \inf_{\substack{p\in\mathbb{R}^{\mathrm{DOF}(p)} \\ p\perp_{\mathbb{M}}\ker(\mathbb{B}^{\mathrm{T}})}}\sup_{\boldsymbol{u}\in\mathbb{R}^{\mathrm{DOF}(\boldsymbol{u})}}\frac{p^{\mathrm{T}}\mathbb{B}\boldsymbol{u}}{(p^{\mathrm{T}}\mathbb{M}p)^{\frac{1}{2}}(\boldsymbol{u}^{\mathrm{T}}\mathbb{A}\boldsymbol{u})^{\frac{1}{2}}} = \inf_{\substack{\hat{p}\in\mathbb{R}^{\mathrm{DOF}(p)} \\ \hat{p}\perp\ker(\mathbb{B}^{\mathrm{T}}\mathbb{M}^{-\frac{1}{2}})}}\sup_{\boldsymbol{u}\in\mathbb{R}^{\mathrm{DOF}(\boldsymbol{u})}}\frac{\hat{p}^{\mathrm{T}}\mathbb{M}^{-\frac{1}{2}}\mathbb{B}\mathbb{A}^{-\frac{1}{2}}\widehat{\boldsymbol{u}}}{(\hat{p}^{\mathrm{T}}\hat{p})^{\frac{1}{2}}(\widehat{\boldsymbol{u}}^{\mathrm{T}}\widehat{\boldsymbol{u}})^{\frac{1}{2}}}$$

$$= \inf_{\substack{p\in\mathbb{R}^{\mathrm{DOF}(p)} \\ \hat{p}\perp\ker(\mathbb{B}^{\mathrm{T}}\mathbb{M}^{-\frac{1}{2}})}}\frac{\hat{p}^{\mathrm{T}}\mathbb{M}^{-\frac{1}{2}}\mathbb{B}\mathbb{A}^{-1}\mathbb{B}^{\mathrm{T}}\mathbb{M}^{-\frac{1}{2}}\hat{p}}{\|\hat{p}\|\|\mathbb{A}^{-\frac{1}{2}}\mathbb{B}^{\mathrm{T}}\mathbb{M}^{-\frac{1}{2}}\hat{p}\|} = \inf_{\substack{p\in\mathbb{R}^{\mathrm{DOF}(p)} \\ \hat{p}\perp\ker(\mathbb{B}^{\mathrm{T}}\mathbb{M}^{-\frac{1}{2}})}}\frac{\big(\hat{p}^{\mathrm{T}}\mathbb{M}^{-\frac{1}{2}}\mathbb{B}\mathbb{A}^{-1}\mathbb{B}^{\mathrm{T}}\mathbb{M}^{-\frac{1}{2}}\hat{p}\big)^{\frac{1}{2}}}{\|\hat{p}\|} = \inf_{\substack{p\in\mathbb{R}^{\mathrm{DOF}(p)} \\ p\perp_{\mathbb{M}}\ker(\mathbb{B}^{\mathrm{T}})}}\frac{\big(p^{\mathrm{T}}\mathbb{B}\mathbb{A}^{-1}\mathbb{B}^{\mathrm{T}}p\big)^{\frac{1}{2}}}{(p^{\mathrm{T}}\mathbb{M}p)^{\frac{1}{2}}}.$$

In other words, β_h can be obtained numerically by computing the smallest non-zero eigenvalue of

(4.2) $$\mathbb{B}\mathbb{A}^{-1}\mathbb{B}^{\mathrm{T}}p = \mu^2\mathbb{M}p, \text{ or equivalently } -\overset{\times}{\nabla}_h^{\prime}\cdot(1 - \overset{\times}{\nabla}_h^{\perp}\overset{\times}{\nabla}_h^{\perp\prime}\cdot - \overset{\times}{\nabla}_h\overset{\times}{\nabla}_h^{\prime}\cdot)^{-1}\overset{\times}{\nabla}_h p = \mu^2 p$$

and $\beta_h = \sqrt{\min\{\mu_i^2|\mu_i^2 > 0\}}$ from (4.1). The computed β_h for GMAC and the schemes mentioned in section 3.5 are summarized in Table 4.1. It is clear that $\beta_h = O(1)$ for both GMACc and GMACg. In contrast, KF, BCG and $Q_1 - P_0$ all result in $\beta_h = O(h)$.

TABLE 4.1
β_h for GMAC and similarly staggered schemes.

# cells	GMACc	BCG	GMACg	KF	$Q_1 - P_0$
32×32	4.924E-1	3.472E-2	4.453E-1	3.432E-2	5.886E-2
64×64	4.774E-1	1.736E-2	4.405E-1	1.726E-2	2.976E-2
128×128	4.669E-1	8.678E-3	4.374E-1	8.654E-3	1.496E-2
256×256	4.593E-1	4.339E-3	4.351E-1	4.333E-3	7.497E-3
512×512	4.536E-1	2.169E-3	4.335E-1	2.168E-3	3.753E-3

Example 2: Convergence Test on a Patched Domain

We proceed with standard accuracy check on a circular domain patched by five non-overlapping coordinate charts as shown in Figure 4.1.

We take the exact solution to be

$$\boldsymbol{u}^e(t,x,y) = \cos(t)\cdot\big(-y(1 - x^2 - y^2), \ x(1 - x^2 - y^2)\big), \quad p^e(t,x,y) = \sin(t)\cdot(1 - x^2 - y^2)$$
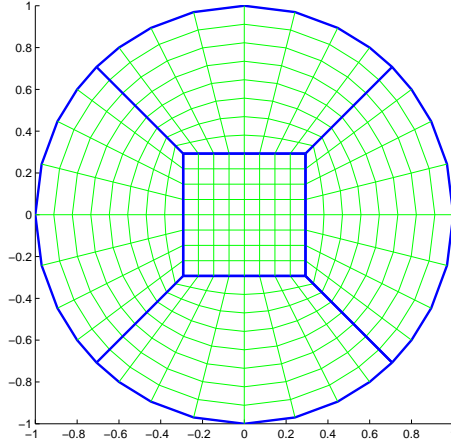
FIG. 4.1. *Domain patched by non-overlapping coordinate charts.*

on the unit disk $\Omega = \{x^2 + y^2 \leq 1\}$ and generate the corresponding forcing term $\boldsymbol{f}$ with $\nu = 1$.

The result at $T = 5.0$ is summarized in Table 4.2. We used semi-implicit time stepping (3.70) with $\Delta t = 5\Delta x$, where $\Delta x = L/N$ is the mesh size in the inner square. Here $L = 1/(1 + \sqrt{2}/2)$ and each coordinate chart is divided into $N \times N$ cells. The result shows clean second order accuracy.

TABLE 4.2
Absolute error and rate of convergence for Example 2.

# cells	$\|\boldsymbol{u}^e - \boldsymbol{u}^h\|_2$	order	$\|\omega^e - \omega^h\|_2$	order	$\|p^e - p^h\|_2$	order
5×16^2	$3.48E-4$		$1.64E-3$		$8.33E-4$	
5×32^2	$8.51E-5$	2.03	$4.01E-4$	2.03	$2.04E-4$	2.03
5×64^2	$2.14E-5$	1.99	$1.01E-4$	1.99	$5.04E-5$	2.02
5×128^2	$5.32E-6$	2.00	$2.51E-5$	2.00	$1.26E-5$	2.01

Example 3: Benchmark Test: Lid-Driven Cavity Flow
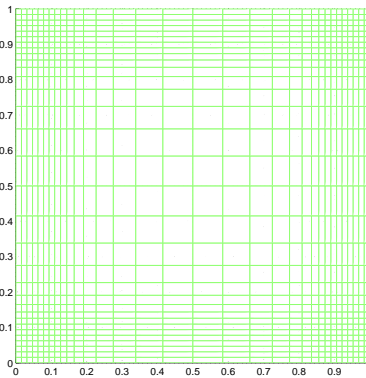

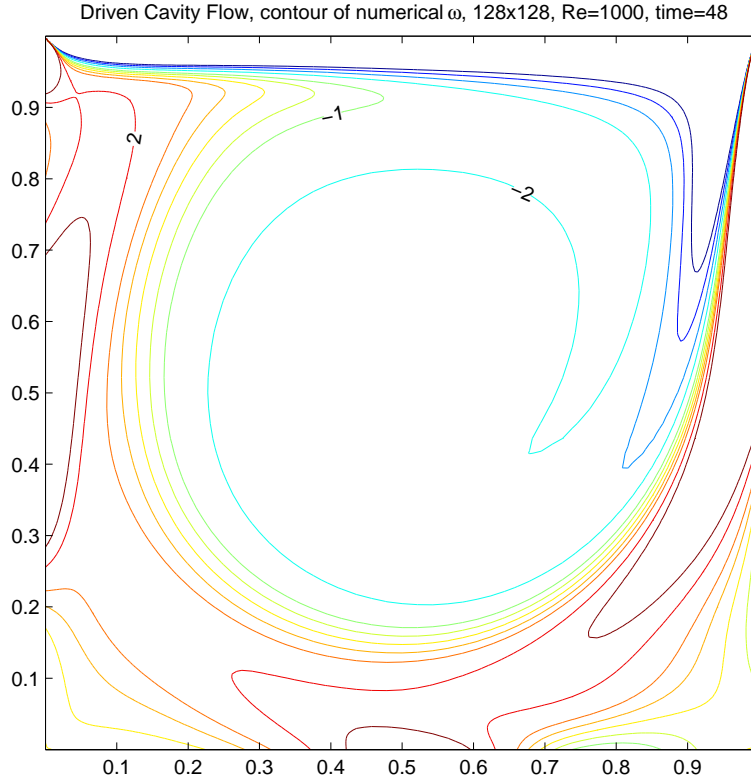FIG. 4.2. *Illustration of the adaptive grid used for the lid-driven cavity flow (Example 3)*

21

Fɪɢ. 4.3. *Vorticity contour plot of the lid-driven cavity flow (Example 3) at Re=1,000.*

We continue with the benchmark problem of lid-driven cavity flow [Bu, GGS, BP]. Here the domain $\Omega = [0,1]^2$. The flow is initially at rest and driven by a slip velocity $\boldsymbol{u} = (1,0)$ on top. The grids are adapted near the boundary to better resolve the flow pattern there. A 32×32 adaptive grid partitioning is shown in Figure 4.2 for illustration. The results for $Re = \frac{1}{\nu} = 1,000$ with 128×128 adaptive grids and $Re = 10,000$ with 180×180 adaptive grids are presented in Figure 4.3 and Figure 4.4 respectively. Both are simulated till $T \approx 1.5\sqrt{Re}$: $T_{1000} = 48.0$, $T_{10000} = 255.0$ using 4th order explicit Runge-Kutta time stepping. The $Re = 1,000$ case agrees well with the benchmark result in [BP].

Example 4: Convergence Test for 3D Cavity Flow with Bottom Topography

In this example, we perform accuracy check for GMAC3Dc-iso on a 3D cavity flow with bottom topography at $Re = 2,000$ with explicit 4th order Runge-Kutta time stepping.

The domain is $[0,1] \times [0,1] \times [g(x,y),1]$ where $g(x,y) = 0.15 \sin(2\pi x)\sin(2\pi y)$ is the bottom topography as shown in Figure 4.5.

We take the exact solution to be $\boldsymbol{u}^e = \nabla \times \boldsymbol{\psi}^e$, $p^e(t,x,y,z) = \cos(t)\cos(x)\sin(y)e^z$ where $\boldsymbol{\psi}^e(t,x,y,z) = \cos(t)(\psi_1^e, \psi_2^e, \psi_3^e)$ and

$$
\begin{aligned}
\psi_1^e(x,y,z) &= \sin^2(\pi x)\sin^2(\pi y)(z-1)^2(z-g(x,y))^2 \\
\psi_2^e(x,y,z) &= \sin^2(\pi x)\sin^2(2\pi y)(z-1)^2(z-g(x,y))^2 \\
\psi_3^e(x,y,z) &= \sin^2(2\pi x)\sin^2(\pi y)(z-1)^2(z-g(x,y))^2
\end{aligned}
$$
(4.3)

The right hand side $\boldsymbol{f}(t,x,y,z)$ is generated accordingly with $\nu = 1/2000$.

The result at $T = 5.0$ is summarized in Table 4.3 and shows second order accuracy.

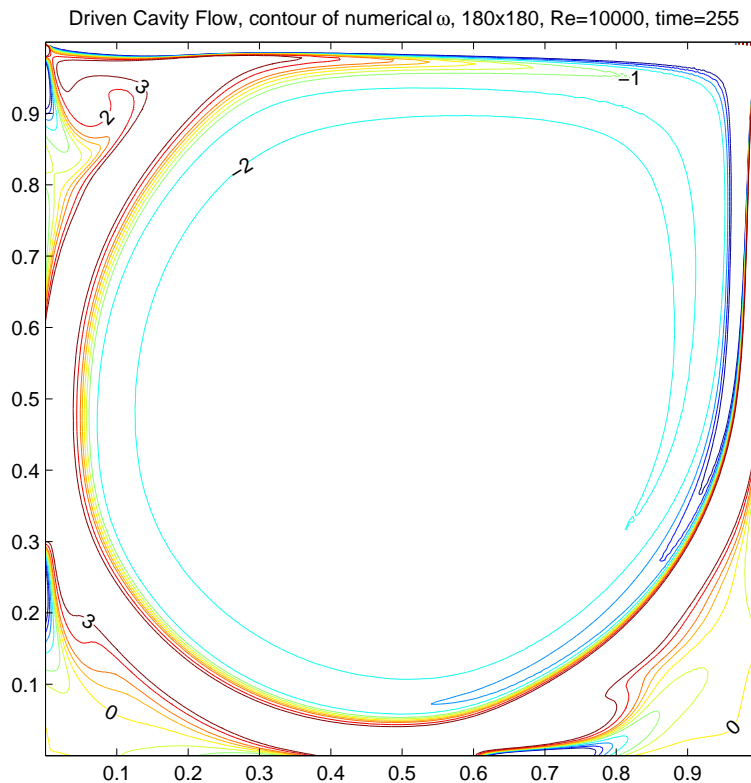Driven Cavity Flow, contour of numerical ω, 180x180, Re=10000, time=255

FIG. 4.4. *Vorticity contour plot of the lid-driven cavity flow (Example 3) at Re=10,000.*

TABLE 4.3
Absolute error and rate of convergence for Example 4.

# cells	$\|\boldsymbol{u}^e - \boldsymbol{u}^h\|_2$	order	$\|\boldsymbol{\omega}^e - \boldsymbol{\omega}^h\|_2$	order	$\|p^e - p^h\|_2$	order
$32 \times 32 \times 32$	$1.95E-2$		$3.84E-1$		$1.06E-3$	
$64 \times 64 \times 64$	$4.91E-3$	1.99	$9.90E-2$	1.96	$2.69E-4$	1.99
$128 \times 128 \times 128$	$1.24E-3$	1.99	$2.51E-2$	1.98	$6.97E-5$	1.95

5. Conclusion. In this paper, we have proposed a novel finite difference scheme for incompressible Navier-Stokes. The main features of the new scheme include:

1. It partially resembles the classical MAC scheme in the sense that velocity and pressure are defined on different locations.
2. It is applicable on general curvilinear domains and easy to implement.
3. The spatial discretization is based on intrinsic differential operators div, grad, curl and is mutually compatible. It naturally incorporates no-slip conditions and is endowed with desirable properties such as summation by parts identities and exact discrete Hodge decomposition. As a result, pressure can be decoupled from the momentum equation without imposing artificial boundary conditions.
4. The pressure Poisson equation is symmetric and semi-definite. Standard fast solvers for large linear systems are applicable.
5. More importantly, the spatial discretization satisfies the inf-sup condition, giving full second order
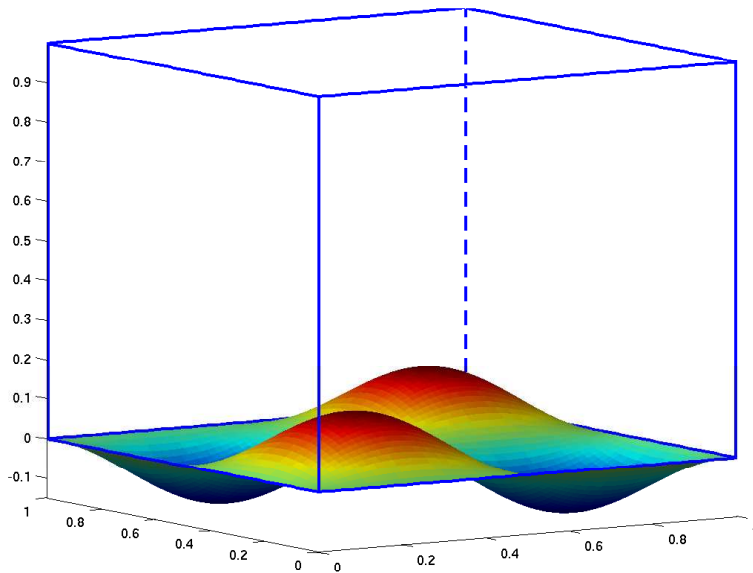
23

Fig. 4.5. *3D cavity with bottom topography*

accuracy for velocity and pressure in both dynamic and steady state calculations.

Systematic numerical experiments are conducted to verify the accuracy and robustness of the proposed scheme.

REFERENCES

[ABCHW] A.S. Almgren, J.B. Bell, P. Colella, L.H. Howell, and M.L. Welcome, A conservative adaptive projection method for the variable density incompressible Navier-Stokes equations. J. Comput. Phy., **142** (1998) 1–46.

[ABCM] A.S. Almgren, J.B. Bell, P. Colella, and T. Marthaler, A Cartesian grid projection method for the incompressible Euler equations in complex geometries. SIAM J. Sci. Comput., **18** (1997) 1289–1309.

[Ar] A. Arakawa, Computational design for long-term numerical integration of the equations of fluid motion: two dimensional incompressible flow. Part I, J. Compute. Phys. **1** (1966) 119-143.

[ArL] A. Arakawa and V. R. Lamb, A potential enstrophy and energy conservation scheme for the shallow water equations, Monthly Weather Review. **109** (1981) 18–36.

[AFW] D. N. Arnold, R. S. Falk and R. Winther, Finite element exterior calculus, homological techniques, and applications, Acta Numerica (2006) 1–155.

[An] C.R. Anderson, Derivation and solution of the discrete pressure equations for the incompressible Navier-Stokes equations, preprint LBL-26353, Lawrence Berkeley Laboratory, Berkeley, CA, 1988.

[BCG] J.B. Bell, P. Colella and H. Glaz, A second-order projection method for the incompressible Navier-Stokes equations, J. Comput. Phys., **85** (1989) 257–283.

[BS] S.C. Brenner and L.R. Scott, The Mathematical Theory of Finite Element Methods, Springer-Verlag, New York, (2002).

[BCM] D. Brown, R. Cortez, M. Minion, Accurate projection methods for the incompressible NavierStokes equations, J. Comput. Phys. **168** (2001) 464–499.

[BD] F. Bertagnolio and O. Daube, Solution of the div-curl problem in generalized curvilinear coordinates, J. Comput. Phys., **138** (1997) 121–152.

[BF] F. Brezzi and M. Fortin, Mixed and Hybrid Finite Element Methods, Springer Series in Computational Mathematics, 15, Springer Verlag, Berlin, 1991.

[BN]   J.M. Boland and R.A. Nicolaides, On the stability of bilinear-constant velocity-pressure finite elements, Numer. Math., **44** (1984) 219–222.

[BP]   O. Botella and R. Peyret, Benchmark spectral results on the lid-driven cavity flow, Comput. & Fluids, **27** (1998) 421–433.

[BR]   M. Braack and T. Richter, Solutions of 3D Navier-Stokes benchmark problems with adaptive finite elements, Computers & fluids, **35** (2006) 372-392.

[BHM]   W. L. Briggs, V. E. Henson, and S. F. McCormick, A Multigrid Tutorial, 2nd ed., SIAM, Philadelphia, 2000.

[Bu]   O. R. Burggraf, Analytical and numerical studies of the structure of steady separated flows, J. Fluid Mech., **24** (1966) 113–151.

[CDHM] P. Colella, M. R. Dorr, J. A. F; Hittinger and D. F. Martin, High-order, finite-volume methods in mapped coordinates. J. Comput. Phys. **230** (2011), 29522976.

[ChH]   Q. Chang and Z. Huang, Efficient algebraic multigrid algorithms and their convergence, SIAM J. Sci. Comput. **24** (2002) 597–618.

[Cho]   S. H. Chou and D. Y. Kwak, Analysis and convergence of a MAC-like scheme for the generalized Stokes problem, Num. Meth. PDE, **13**, (1997)147–163.

[DHSW] B.J. Daly, F.H. Harlow, J.P. Shannon, and J.E. Welch, The MAC scheme, Tech. report LA-3425, Los Alamos Scientific Laboratory, University of California, 1965.

[DFM]   M.O. Deville, P.F. Fischer, E.H. Mund High-Order Methods for Incompressible Fluid Flow, Cambridge University Press, 2002

[EL]   W. E and J.-G. Liu, Vorticity boundary condition and related issues for finite difference schemes, J. Comput. Phys., **124** (1996) 368–382.

[ESW]   H.C. Elman, D.J. Silvester and A.J. Wathen, Finite Elements and Fast Iterative Solvers: with Applications in Incompressible Fluid Dynamics, Oxford University Press, 2005

[FPT]   M. Fortin, R. Peyret and R. Temam, Résolution numérique des équations de Navier-Stokes pour un fluide incompressible, J. Mécanique, **10** (1971) 357–390.

[FP]   J.H. Ferziger, M. Peric, Computational Methods for Fluid Dynamics, 3rd edition, Springer, 2001

[GGS]   U. Ghia, K. N. Ghia and C. T. Shin, High-Re solutions for incompressible flow using the Navier-Stokes equations and a multigrid method, J. Comput. Phys., **48** (1982) 387–411.

[GR]   V. Girault and P.A. Raviart, Finite Element Methods for Navier-Stokes Equations: Theory and Algorithms, Springer-Verlag, New York, (1986).

[GS]   P.M. Gresho and R.L. Sani, Incompressible Flow and the Finite Element Method, Volume 1, Advection-Diffusion and Isothermal Laminar Flow, Wiley, 2001

[GeS]   L. Ge and F. Sotiropoulos, A numerical method for solving the 3D unsteady incompressible Navier-Stokes equations in curvilinear domains with complex immersed boundaries. J. Comput. Phys. **225** (2007), 17821809.

[GMS]   J.-L. Guermond, P. Minev and J. Shen, An overview of projection methods for incompressible flows. Comp. Meth. Appl. Mech. Engng., **195** (2006) 6011–6045.

[Han]   H. Han, Nonconforming elements in the mixed finite element method. J. Comp. Math., **2** (1984) 223-233.

[HWu]   H. Han and X. Wu, A new mixed finite element formulation and the MAC method for the Stokes equations, SIAM J. Num. Anal., **35** (1998) 560–571.

[HY]   H.D. Han and M. Yan, A mixed finite element method on a staggered mesh for Navier-Stokes equation, J. Comp. Math. **26** (2008) 816–824.,

[HoW]   T.Y. Hou and B.T.R. Wetton, Second-order convergence of a projection scheme for the incompressible Navier-Stokes equations with boundaries, SIAM. J. Num. Anal., **30** (1993) 609–629.

[HLW]   Y.-L. Huang, J.-G. Liu and W.-C. Wang, Error analysis of the generalized MAC scheme, Preprint `http://www.math.nthu.edu.tw/~wangwc/research/research.html`.

[HWa]   Y.-L. Huang, W.-C. Wang, Adaptive Computation of the corner singularity with the monotone jump condition capturing scheme. Recent advances in adaptive computation, Contemp. Math., **383** (2005) 253–267.

[HS]   J.M. Hyman and M. Shashkov, Natural discretizations for the divergence, gradient, and curl on logically rectangular grids, Comput. Math. Appl. **33**, (1997) 81-104.

[KK]   G.E. Karniadakis and R.M. Kirby II, Parallel Scientific Computing in C++ and MPI: A Seamless Approach to Parallel Algorithms and their Implementation, Cambridge University Press, 2003

[KS]   G.E. Karniadakis and S.J. Sherwin, Spectral/hp Element Methods for Computational Fluid Dynamics, 2nd edition, Oxford University Press, 2005

[Ku]   B.G. Kuznetsov, Numerical methods for solving some problems of viscous liquid, Fluid Dynam. Trans., **4** (1968) 85–89.

[Le]   V.L. Lebedev, Difference analogues of orthogonal decompositions, fundamental differential operators and certain boundary-value problems of mathematical physics, Z. Vycisl. Mat. i Mat. Fiz., **4** (1964) 449–465 (in Russian).

[LLP]   J.-G. Liu, J. Liu and R. Pego, Stability and convergence of efficient Navier-Stokes solvers via a commutator estimate, Comm. Pure Appl. Math., **60** (2007) 1443–1487.

[HW]   F.H. Harlow and J.E. Welch, Numerical calculation of time-dependent viscous incompressible flow of fluid with free surface, Phys. Fluids, **8** (1965) 2182–2189.

[LB]   H. Luo and T. R. Bewley, On the contravariant form of the Navier-Stokes equations in time-dependent curvilinear

coordinate systems. J. Comput. Phys. **199** (2004), 355375.

[LWa]   J.-G. Liu and W.C. Wang, Energy and helicity preserving schemes for hydro- and magnetohydro-dynamics flows with symmetry, J. Comput. Phys., **200** (2004), pp. 8–33.

[NC]   J. Nordström and M. H. Carpenter, High-order finite difference methods, multidimensional linear problems, and curvilinear coordinates, J. Comput. Phy. **173** (2001) 149–174.

[OOB]   L.H. Olesen, F. Okkels and H. Bruus, A high level programming language implementation of topology optimization applied to steady state Navier-Stokes flow. International Journal for Numerical Methods in Engineering, **65** (2006) 975-1001.

[OI]   S.A. Orszag and M. Israeli, Numerical simulation of viscous incompressible flows, Annu. Rev. Fluid Mech., **6** (1974) 281–318.

[OID]   S.A. Orszag, M. Israeli and M. Deville, Boundary conditions for incompressible flows, J. Sci. Comput., **1** (1986) 75–111.

[PT]   R. Peyret and T.D. Taylor, Computational Methods for Fluid Flow, Springer-Verlag, New York, (1983)

[RaTu]   R. Ranacher and S. Turek, Simple non-conforming quadrilateral Stokes element, Num. Meth. PDE. **8** (1992) 97-112.

[RBLCB]   C.A. Rendleman, V.E. Beckner, M. Lijewski, W. Crutchfield, and J.B. Bell, Parallelization of structured, hierarchical adaptive mesh refinement algorithms Computing and Visualization in Science, **3** (2000) 147–157.

[TW]   A. Toselli and O. Widlund, Domain Decomposition Methods - Algorithms and Theory, Springer, 2005

[TC]   D. P. Trebotich and P. Colella, A projection method for incompressible viscous flow on moving quadrilateral grids, J. Comput. Phys., **166** (2001), 191–217.

[TOS]   U. Trottenberg, C. W. Oosterlee, and A. Schüller, Multigrid, Academic Press, San Diego, CA, 2001.

[Wa]   W.-C. Wang, A jump condition capturing finite difference scheme for elliptic interface problems, SIAM J. Sci. Comput., **25** (2004) 1479–1496.

[We]   B.R. Wetton, Analysis of the spatial error for a class of finite difference methods for viscous incompressible flow, SIAM J. Num. Anal., **34** (1997) 723–755.

[ZSK]   Y. Zang, R. L. Street, and J. R. Koseff A Non-staggered Grid, Fractional Step Method for Time-Dependent Incompressible Navier-Stokes Equations in Curvilinear Coordinates, J. Comput. Phys., **114** (1994), 18–33.

Appendix A. GMACg, Another Version of Generalized MAC Scheme.

An alternative placement of the unknown variables

$$(A.1) \qquad\qquad \boldsymbol{u} \in L^2(\mathring{\Omega}_{\mathrm{g}}, \mathbb{R}^2), \qquad p,\ \omega \in L^2(\Omega_{\mathrm{c}}, \mathbb{R})$$

leads to a variant of the scheme (3.44). In this setting, we place both components of the velocity on grid points, pressure and vorticity on cell centers. Note that the boundary velocity $\boldsymbol{u}_b \in L^2(\Gamma_{\mathrm{g}}, \mathbb{R}^2)$ is prescribed data and not listed in (A.1) as part of active variables.

Associated with this new placements are the following function spaces

$$(A.2) \quad L^2(\mathring{\Omega}_{\mathrm{g}}, \mathbb{R}^2) := \{\boldsymbol{u} : \mathring{\Omega}_{\mathrm{g}} \to \mathbb{R}^2\}, \quad L^2(\Gamma_{\mathrm{g}}, \mathbb{R}^2) := \{\boldsymbol{u}_b : \Gamma_g \to \mathbb{R}^2\}, \quad L^2(\Omega_{\mathrm{c}}, \mathbb{R}) := \{a : \Omega_{\mathrm{c}} \to \mathbb{R}\}.$$

and finite difference operators

$$(A.3) \qquad\qquad \overset{\times}{\nabla}{}^{\circ}_h : L^2(\Omega_{\mathrm{c}}, \mathbb{R}) \mapsto L^2(\mathring{\Omega}_{\mathrm{g}}, \mathbb{R}), \qquad \overset{\times}{\nabla}{}^{\circ}_h p := (\overset{\times}{D}_1 p)\,\overset{\times}{\boldsymbol{e}}{}^1 + (\overset{\times}{D}_2 p)\,\overset{\times}{\boldsymbol{e}}{}^2 \qquad \text{on } \mathring{\Omega}_{\mathrm{g}};$$

$$(A.4) \qquad\qquad \overset{\times}{\nabla}{}^{\circ\perp}_h : L^2(\Omega_{\mathrm{c}}, \mathbb{R}) \mapsto L^2(\mathring{\Omega}_{\mathrm{g}}, \mathbb{R}), \qquad \overset{\times}{\nabla}{}^{\circ\perp}_h \omega := \frac{-\overset{\times}{D}_2 \omega}{\sqrt{\overset{\times}{g}_h}}\overset{\times}{\boldsymbol{e}}_1 + \frac{\overset{\times}{D}_1 \omega}{\sqrt{\overset{\times}{g}_h}}\overset{\times}{\boldsymbol{e}}_2 \qquad \text{on } \mathring{\Omega}_{\mathrm{g}}.$$

Note that the operators $\overset{\times}{\nabla}{}^{\circ}_h$ and $\overset{\times}{\nabla}{}^{\circ\perp}_h$ are exactly the standard finite difference operators as (3.29) and (3.30), except (A.3) and (A.4) are defined for vector fields on Ω_{c}. We use the superscript '$\circ$' to emphasize that $\overset{\times}{\nabla}{}^{\circ}_h$ and $\overset{\times}{\nabla}{}^{\circ\perp}_h$ are 'interior' gradient operators whose range are vector fields defined only on the interior grids.

For inhomogeneous boundary velocity, the operators $\overset{\times}{\nabla}{}^{\circ\prime}_h \cdot$ and $\overset{\times}{\nabla}{}^{\circ\perp\prime}_h \cdot$ involve both the active variable $\boldsymbol{u} \in L^2(\mathring{\Omega}_{\mathrm{g}}, \mathbb{R}^2)$ and the data $\boldsymbol{u}_b \in L^2(\Gamma_{\mathrm{g}}, \mathbb{R}^2)$. Denote by $\boldsymbol{U} = \boldsymbol{u} \oplus \boldsymbol{u}_b$, that is

$$(A.5) \qquad\qquad \overset{\times}{U}{}^{\alpha} = \begin{cases} \overset{\times}{u}{}^{\alpha} & \text{on } \mathring{\Omega}_{\mathrm{g}}, \\ \overset{\times}{u}{}^{\alpha}_b & \text{on } \Gamma_g, \end{cases} \quad \overset{\times}{U}_{\alpha} = \begin{cases} \overset{\times}{u}_{\alpha} & \text{on } \mathring{\Omega}_{\mathrm{g}}, \\ (\overset{\times}{u}_b)_{\alpha} & \text{on } \Gamma_g, \end{cases} \quad \alpha = 1, 2,$$

we define

$$(A.6) \quad \overset{\times}{\nabla}{}^{\circ\prime}_h \cdot : L^2(\mathring{\Omega}_{\mathrm{g}}, \mathbb{R}^2) \oplus L^2(\Gamma_{\mathrm{g}}, \mathbb{R}^2) \mapsto L^2(\Omega_{\mathrm{c}}, \mathbb{R}), \quad \overset{\times}{\nabla}{}^{\circ\prime}_h \cdot (\boldsymbol{u} \oplus \boldsymbol{u}_b) = \frac{1}{\sqrt{\overset{\times}{g}_h}}\left(\overset{\times}{D}_1(\sqrt{\overset{\times}{g}_h}\,\overset{\times}{U}{}^1) + \overset{\times}{D}_2(\sqrt{\overset{\times}{g}_h}\,\overset{\times}{U}{}^2)\right)$$

$$(A.7) \quad \overset{\times}{\nabla}{}^{\circ\perp\prime}_h \cdot : L^2(\mathring{\Omega}_{\mathrm{g}}, \mathbb{R}^2) \oplus L^2(\Gamma_{\mathrm{g}}, \mathbb{R}^2) \mapsto L^2(\Omega_{\mathrm{c}}, \mathbb{R}), \quad \overset{\times}{\nabla}{}^{\circ\perp\prime}_h \cdot (\boldsymbol{u} \oplus \boldsymbol{u}_b) = \frac{1}{\sqrt{\overset{\times}{g}_h}}(\overset{\times}{D}_1 \overset{\times}{U}_2 - \overset{\times}{D}_2 \overset{\times}{U}_1)$$
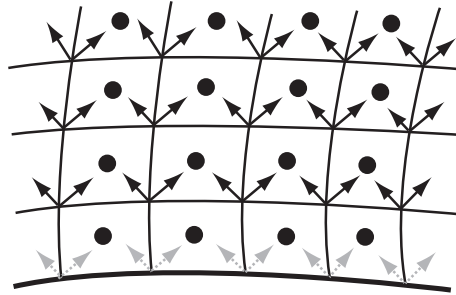

FIG. A.1. *Positions of velocity field ($\nwarrow$ and $\nearrow$), vorticity and pressure ($\bullet$) for the scheme* (A.17).

As before, for $\boldsymbol{u} \in L^2(\mathring{\Omega}_{\mathrm{g}}, \mathbb{R}^2)$,

$$(\text{A.8}) \qquad \overset{\times}{\nabla}_h^{\circ\prime} \cdot \boldsymbol{u} := \overset{\times}{\nabla}_h^{\circ\prime} \cdot (\boldsymbol{u} \oplus \boldsymbol{0}), \quad \overset{\times}{\nabla}_h^{\circ\perp\prime} \cdot \boldsymbol{u} := \overset{\times}{\nabla}_h^{\circ\perp\prime} \cdot (\boldsymbol{u} \oplus \boldsymbol{0}).$$

Finally,

$$(\text{A.9}) \qquad \overset{\times}{\triangle}_h^{\circ\prime} : L^2(\Omega_{\mathrm{c}}, \mathbb{R}) \mapsto L^2(\Omega_{\mathrm{c}}, \mathbb{R}), \qquad \overset{\times}{\triangle}_h^{\circ\prime} p = \overset{\times}{\nabla}_h^{\circ\prime} \cdot \overset{\times}{\nabla}_h^{\circ} p = \overset{\times}{\nabla}_h^{\circ\prime} \cdot \left((\overset{\times}{\nabla}_h^{\circ} p) \oplus \boldsymbol{0} \right).$$

Define the discrete inner products

$$(\text{A.10}) \qquad \langle\, \boldsymbol{u} \,,\, \boldsymbol{v} \,\rangle_{\mathring{\Omega}_{\mathrm{g}}} = h_1 h_2 \sum_{i=1}^{M-1} \sum_{j=1}^{N-1} \left((\boldsymbol{u} \cdot \boldsymbol{v}) \sqrt{g_h} \right)_{i,j}, \qquad \boldsymbol{u},\, \boldsymbol{v} \in L^2(\mathring{\Omega}_{\mathrm{g}}, \mathbb{R}^2),$$

$$(\text{A.11}) \qquad \langle\, a \,,\, b \,\rangle_{\Omega_{\mathrm{c}}} = h_1 h_2 \sum_{i=1}^{M} \sum_{j=1}^{N} \left(a\, b\, \sqrt{g_h} \right)_{i-\frac{1}{2}, j-\frac{1}{2}}, \qquad a,\, b \in L^2(\Omega_{\mathrm{c}}, \mathbb{R}).$$

The counterpart of Lemma 3.1 is also valid:

LEMMA A.1. *If* $\boldsymbol{u} \in L^2(\mathring{\Omega}_{\mathrm{g}}, \mathbb{R}^2)$ *and* $a \in L^2(\Omega_{\mathrm{c}}, \mathbb{R})$. *Then we have*

1.

$$(\text{A.12}) \qquad \langle\, \boldsymbol{u} \,,\, \overset{\times}{\nabla}_h^{\circ} a \,\rangle_{\mathring{\Omega}_{\mathrm{g}}} = -\langle\, \overset{\times}{\nabla}_h^{\circ\prime} \cdot \boldsymbol{u} \,,\, a \,\rangle_{\Omega_{\mathrm{c}}}$$

2.

$$(\text{A.13}) \qquad \langle\, \boldsymbol{u} \,,\, \overset{\times}{\nabla}_h^{\circ\perp} a \,\rangle_{\mathring{\Omega}_{\mathrm{g}}} = -\langle\, \overset{\times}{\nabla}_h^{\circ\perp\prime} \cdot \boldsymbol{u} \,,\, a \,\rangle_{\Omega_{\mathrm{c}}}$$

3.

$$(\text{A.14}) \qquad \overset{\times}{\nabla}_h^{\circ\prime} \cdot (\overset{\times}{\nabla}_h^{\circ} a) = \overset{\times}{\nabla}_h^{\circ\perp\prime} \cdot (\overset{\times}{\nabla}_h^{\circ\perp} a) = \overset{\times}{\triangle}_h^{\circ\prime} a \quad \text{on } \Omega_{\mathrm{c}};$$

4. *If* $a \in L^2(\Omega_{\mathrm{c}}, \mathbb{R})$, *then*

$$(\text{A.15}) \qquad \overset{\times}{\nabla}_h^{\circ\prime} \cdot (\overset{\times}{\nabla}_h^{\circ\perp} a) = \overset{\times}{\nabla}_h^{\circ\perp\prime} \cdot (\overset{\times}{\nabla}_h^{\circ} a) = 0 \quad \text{on } \mathring{\Omega}_{\mathrm{c}},$$

where $\mathring{\Omega}_{\mathrm{c}} = \left\{ \boldsymbol{x}(\xi_{i-\frac{1}{2}}^1, \xi_{j-\frac{1}{2}}^2) \in \Omega_{\mathrm{c}} : 2 \leq i \leq M-1, 2 \leq j \leq N-1 \right\}$. *If in addition, a is constant on* $\Omega_{\mathrm{c}} \setminus \mathring{\Omega}_{\mathrm{c}}$, *then*

$$(\text{A.16}) \qquad \overset{\times}{\nabla}_h^{\circ\prime} \cdot (\overset{\times}{\nabla}_h^{\circ\perp} a) = \overset{\times}{\nabla}_h^{\circ\perp\prime} \cdot (\overset{\times}{\nabla}_h^{\circ} a) = 0 \quad \text{on } \Omega_{\mathrm{c}}.$$

The generalized MAC scheme with $\boldsymbol{u}$ defined on grids (GMACg) is given by:

The GMACg Scheme:

Solve for $\boldsymbol{u} \in C^1\left([0,T]; L^2(\mathring{\Omega}_{\mathrm{g}}, \mathbb{R}^2)\right)$ and $p \in C^0\left([0,T]; L^2(\Omega_{\mathrm{c}}, \mathbb{R})\right)$ such that

$$(\text{A.17}) \qquad \begin{aligned}
\boldsymbol{u}_t + \bar{\omega} \boldsymbol{u}^\perp + \overset{\times}{\nabla}_h^{\circ} p &= \nu \overset{\times}{\nabla}_h^{\circ\perp} \omega + \boldsymbol{f} & \text{on } \mathring{\Omega}_{\mathrm{g}} \\
\omega &= \overset{\times}{\nabla}_h^{\circ\perp\prime} \cdot (\boldsymbol{u} \oplus \boldsymbol{u}_b) & \text{on } \Omega_{\mathrm{c}} \\
\overset{\times}{\nabla}_h^{\circ\prime} \cdot (\boldsymbol{u} \oplus \boldsymbol{u}_b) &= 0 & \text{on } \Omega_{\mathrm{c}}
\end{aligned}$$

The compatibility condition for the boundary velocity $\boldsymbol{u}_b$ is

$$(\text{A.18}) \qquad \langle\, \boldsymbol{1}_{\Omega_{\mathrm{c_e}}} \,,\, \overset{\times}{\nabla}_h^{\circ\prime} \cdot (\boldsymbol{0} \oplus \boldsymbol{u}_b) \,\rangle_{\Omega_{\mathrm{c}}} = 0 = \langle\, \boldsymbol{1}_{\Omega_{\mathrm{c_o}}} \,,\, \overset{\times}{\nabla}_h^{\circ\prime} \cdot (\boldsymbol{0} \oplus \boldsymbol{u}_b) \,\rangle_{\Omega_{\mathrm{c}}},$$

where

(A.19) $\qquad \Omega_{c_e} := \big\{ \boldsymbol{x}(\xi^1_{i-\frac{1}{2}}, \xi^2_{j-\frac{1}{2}}) \in \Omega_c,\ i+j \text{ is even} \big\}, \quad \Omega_{c_o} := \big\{ \boldsymbol{x}(\xi^1_{i-\frac{1}{2}}, \xi^2_{j-\frac{1}{2}}) \in \Omega_c,\ i+j \text{ is odd} \big\}.$

Furthermore,

(A.20) $$\ker(\overset{\times}{\triangle}{}_h^{\circ\prime}) = \ker(\overset{\times}{\nabla}{}_h^{\circ}) = \operatorname{span}\{\mathbf{1}_{\Omega_{c_e}}, \mathbf{1}_{\Omega_{c_o}}\}.$$

Appendix B. The GMAC3D Scheme.

Generalization of GMAC to 3D with the semi-staggered variable placement as either

(B.1) $\qquad \text{GMAC3Dc}: \quad \boldsymbol{u} \in L^2(\Omega_c, \mathbb{R}^3), \qquad p \in L^2(\bar{\Omega}_g, \mathbb{R}), \qquad \boldsymbol{\omega} \in L^2(\bar{\Omega}_g, \mathbb{R}^3).$

or

(B.2) $\qquad \text{GMAC3Dg}: \quad \boldsymbol{u} \in L^2(\mathring{\Omega}_g, \mathbb{R}^3), \qquad p \in L^2(\Omega_c, \mathbb{R}), \qquad \boldsymbol{\omega} \in L^2(\Omega_c, \mathbb{R}^3).$

are both straightforward once a skewed coordinate system is chosen. We only elaborate on GMAC3Dc.

Take, for example, $(\overset{\vee}{\xi}{}^1, \overset{\vee}{\xi}{}^2, \overset{\vee}{\xi}{}^3)$ as shown in left-top corner of Figure B.1:

(B.3)
$$\begin{aligned}
\overset{\vee}{\xi}{}^1 &:= \frac{h_3\xi^2 + h_2\xi^3}{\sqrt{h_2^2 + h_3^2}}, & \overset{\vee}{h}_1 &= \Delta\overset{\vee}{\xi}{}^1 = \frac{2h_2 h_3}{\sqrt{h_2^2 + h_3^2}} \\
\overset{\vee}{\xi}{}^2 &:= \frac{h_1\xi^3 + h_3\xi^1}{\sqrt{h_3^2 + h_1^2}}, & \overset{\vee}{h}_2 &= \Delta\overset{\vee}{\xi}{}^2 = \frac{2h_3 h_1}{\sqrt{h_3^2 + h_1^2}} \\
\overset{\vee}{\xi}{}^3 &:= \frac{h_2\xi^1 + h_1\xi^2}{\sqrt{h_1^2 + h_2^2}}, & \overset{\vee}{h}_3 &= \Delta\overset{\vee}{\xi}{}^3 = \frac{2h_1 h_2}{\sqrt{h_1^2 + h_2^2}}
\end{aligned}$$

The discrete metric tensors $\{\overset{\vee}{g}{}^h_{\alpha\beta}\}_{\alpha,\beta=1}^3$, $\{\overset{\vee}{g}{}_h^{\alpha\beta}\}_{\alpha,\beta=1}^3$ and $\sqrt{\overset{\vee}{g}_h}$ with respect to $(\overset{\vee}{\xi}{}^1, \overset{\vee}{\xi}{}^2, \overset{\vee}{\xi}{}^3)$ as well as the reduced difference operators $\overset{\vee}{D}{}'_\alpha$ and $\overset{\vee}{D}_\alpha$ can be defined in a similar way as in the 2D case.

We therefore arrive at the first version of our scheme for 3D Navier-Stokes equation (3.1):

The GMAC3Dc-skew Scheme:

Solve for $\boldsymbol{u} \in C^1\big([0,T]; L^2(\Omega_c, \mathbb{R}^3)\big)$ and $p \in C^0\big([0,T]; L^2(\mathring{\Omega}_g, \mathbb{R})\big)$ such that

(B.4)
$$\begin{aligned}
\boldsymbol{u}_t + \bar{\boldsymbol{\omega}} \times \boldsymbol{u} + \overset{\vee}{\nabla}_h p &= \nu\overset{\vee}{\nabla}_h \times \boldsymbol{\omega} + \boldsymbol{f} & &\text{on } \Omega_c \\
\boldsymbol{\omega} &= \overset{\vee}{\nabla}{}'_h \times \boldsymbol{u} & &\text{on } \bar{\Omega}_g \\
\overset{\vee}{\nabla}{}'_h \cdot \boldsymbol{u} &= 0 & &\text{on } \bar{\Omega}_g
\end{aligned}$$

where

(B.5) $\qquad \overset{\vee}{\nabla}_h : L^2(\bar{\Omega}_g, \mathbb{R}) \mapsto L^2(\Omega_c, \mathbb{R}^3), \quad \overset{\vee}{\nabla}_h p := (\overset{\vee}{D}_1 p)\overset{\vee}{\boldsymbol{e}}{}^1 + (\overset{\vee}{D}_2 p)\overset{\vee}{\boldsymbol{e}}{}^2 + (\overset{\vee}{D}_3 p)\overset{\vee}{\boldsymbol{e}}{}^3,$

(B.6) $\qquad \overset{\vee}{\nabla}{}'_h \cdot : L^2(\Omega_c, \mathbb{R}^3) \mapsto L^2(\bar{\Omega}_g, \mathbb{R}), \quad \overset{\vee}{\nabla}{}'_h \cdot \boldsymbol{u} := \frac{1}{\sqrt{\overset{\vee}{g}_h}}\Big(\sum_{\alpha=1}^3 \overset{\vee}{D}{}'_\alpha(\sqrt{\overset{\vee}{g}_h}\overset{\vee}{u}{}^\alpha)\Big),$

(B.7) $\qquad \overset{\vee}{\nabla}{}'_h \times : L^2(\Omega_c, \mathbb{R}^3) \mapsto L^2(\bar{\Omega}_g, \mathbb{R}^3), \quad \overset{\vee}{\nabla}{}'_h \times \boldsymbol{u} := \frac{1}{\sqrt{\overset{\vee}{g}_h}}\begin{vmatrix} \overset{\vee}{\boldsymbol{e}}_1 & \overset{\vee}{\boldsymbol{e}}_2 & \overset{\vee}{\boldsymbol{e}}_3 \\ \overset{\vee}{D}{}'_1 & \overset{\vee}{D}{}'_2 & \overset{\vee}{D}{}'_3 \\ \overset{\vee}{u}_1 & \overset{\vee}{u}_2 & \overset{\vee}{u}_3 \end{vmatrix},$

(B.8) $\qquad \overset{\vee}{\nabla}_h \times : L^2(\bar{\Omega}_g, \mathbb{R}^3) \mapsto L^2(\Omega_c, \mathbb{R}^3), \quad \overset{\vee}{\nabla}_h \times \boldsymbol{\omega} := \frac{1}{\sqrt{\overset{\vee}{g}_h}}\begin{vmatrix} \overset{\vee}{\boldsymbol{e}}_1 & \overset{\vee}{\boldsymbol{e}}_2 & \overset{\vee}{\boldsymbol{e}}_3 \\ \overset{\vee}{D}_1 & \overset{\vee}{D}_2 & \overset{\vee}{D}_3 \\ \overset{\vee}{\omega}_1 & \overset{\vee}{\omega}_2 & \overset{\vee}{\omega}_3 \end{vmatrix},$
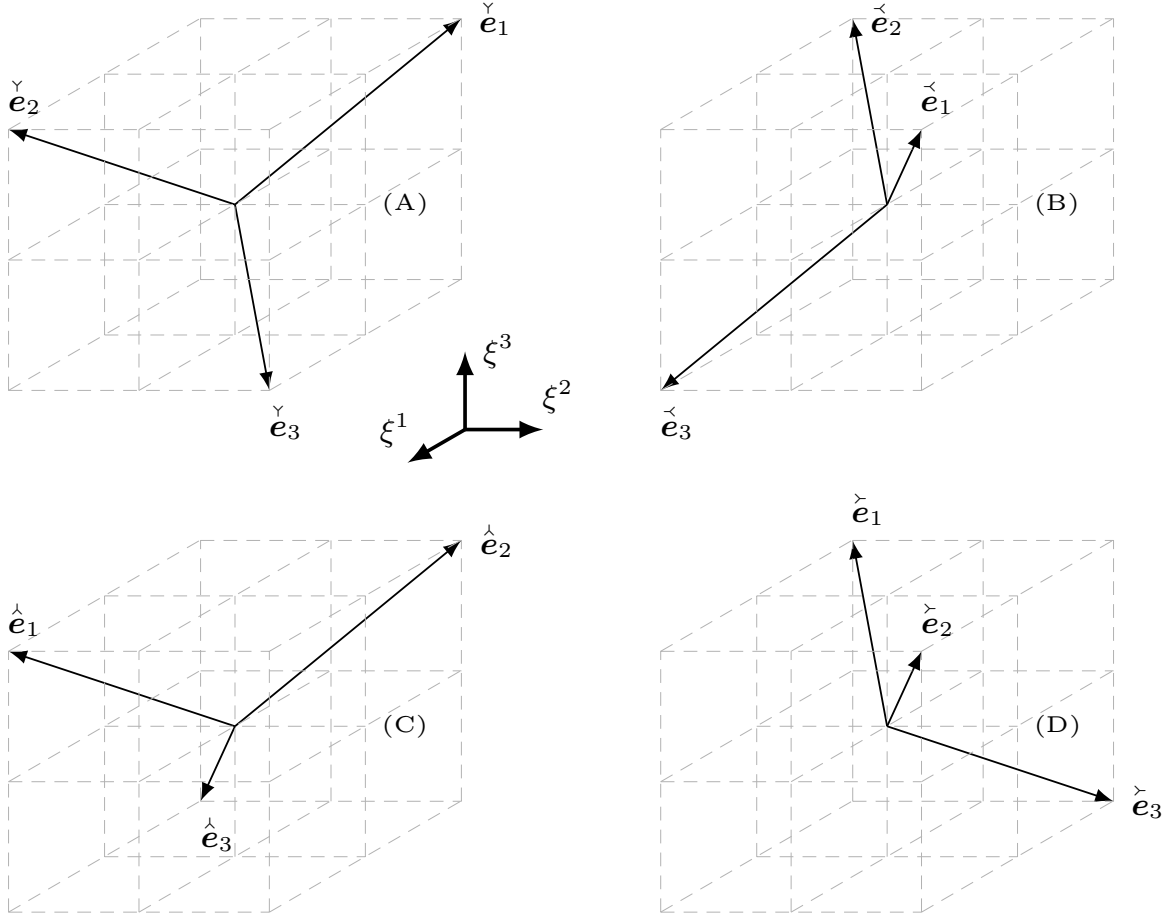
Fig. B.1.

and

$$(B.9) \qquad \overset{\curlyvee}{\triangle}{}'_h : L^2(\bar{\Omega}_\mathrm{g}, \mathbb{R}) \mapsto L^2(\bar{\Omega}_\mathrm{g}, \mathbb{R}), \quad \overset{\curlyvee}{\triangle}{}'_h p = \frac{1}{\sqrt{\overset{\curlyvee}{g}_h}} \sum_{\mu,\nu=1}^{3} \overset{\curlyvee}{D}{}'_\mu \left(\sqrt{\overset{\curlyvee}{g}_h} \overset{\curlyvee}{g}_h^{\mu\nu} \overset{\curlyvee}{D}_\nu p \right).$$

Alternatively, one could have chosen $\{\overset{\curlyvee}{\xi}{}^\alpha\}_{\alpha=1}^3$, $\{\overset{\wedge}{\xi}{}^\alpha\}_{\alpha=1}^3$, or $\{\overset{\curlyvee}{\xi}{}^\alpha\}_{\alpha=1}^3$ as coordinates and discretized accordingly (Figure B.1).

The resulting schemes differ from each other slightly. It should be noted that the averaged version of the four skew operators, for example,

$$(B.10) \qquad \bar{\nabla}_h p := \frac{1}{4}(\overset{\curlyvee}{\nabla}_h p + \overset{\curlyvee}{\nabla}_h p + \overset{\wedge}{\nabla}_h p + \overset{\curlyvee}{\nabla}_h p)$$

is isotropic, or more precisely, invariant under the coordinate transformation $(\xi^1, \xi^2, \xi^3) \mapsto (\xi^2, \xi^3, \xi^1)$. We thus also propose the following isotropic version of the 3D scheme and elaborate with more details below.

30

We first give an alternative expression for the isotropic gradient operator. To this end, we define the following operators with respect to the default coordinate $\{\xi^1, \xi^2, \xi^3\}$:

$$\text{(B.11)} \qquad \bar{D}_1 := D_1 A_2 A_3 : L^2(\bar{\Omega}_{\mathrm{g}}, \mathbb{R}) \to L^2(\Omega_{\mathrm{c}}, \mathbb{R}),$$

$$\text{(B.12)} \qquad \bar{D}_2 := D_2 A_3 A_1 : L^2(\bar{\Omega}_{\mathrm{g}}, \mathbb{R}) \to L^2(\Omega_{\mathrm{c}}, \mathbb{R}),$$

$$\text{(B.13)} \qquad \bar{D}_3 := D_3 A_1 A_2 : L^2(\bar{\Omega}_{\mathrm{g}}, \mathbb{R}) \to L^2(\Omega_{\mathrm{c}}, \mathbb{R}),$$

$$\text{(B.14)} \qquad \bar{D}_1' := D_1' A_2' A_3' : L^2(\Omega_{\mathrm{c}}, \mathbb{R}) \to L^2(\bar{\Omega}_{\mathrm{g}}, \mathbb{R}),$$

$$\text{(B.15)} \qquad \bar{D}_2' := D_2' A_3' A_1' : L^2(\Omega_{\mathrm{c}}, \mathbb{R}) \to L^2(\bar{\Omega}_{\mathrm{g}}, \mathbb{R}),$$

$$\text{(B.16)} \qquad \bar{D}_3' := D_3' A_1' A_2' : L^2(\Omega_{\mathrm{c}}, \mathbb{R}) \to L^2(\bar{\Omega}_{\mathrm{g}}, \mathbb{R}).$$

where D is the standard short-stencil finite difference operator, D' is the reduced finite difference operator as defined in (3.11), and the averaging operators are defined by

$$\text{(B.17)} \qquad (Ag)_{i-\frac{1}{2}} = \frac{1}{2}(g_i + g_{i-1}), \quad 1 \le i \le N, \qquad (A'f)_i = \begin{cases} f_{\frac{1}{2}} & i = 0 \\ \frac{1}{2}(f_{i+\frac{1}{2}} + f_{i-\frac{1}{2}}) & 1 \le i \le N-1 \\ f_{N-\frac{1}{2}} & i = N \end{cases}$$

With lengthy but elementary calculations, it can be shown that the isotropic gradient defined in (B.10) can be recast in terms of the operators in the default coordinate

$$\text{(B.18)} \qquad \bar{\nabla}_h p = (\bar{D}_1 p)\boldsymbol{e}^1 + (\bar{D}_2 p)\boldsymbol{e}^2 + (\bar{D}_3 p)\boldsymbol{e}^3 \in L^2(\Omega_{\mathrm{c}}, \mathbb{R}^3).$$

where $\boldsymbol{e}^\alpha = \nabla \xi^\alpha$, $\boldsymbol{e}_\alpha = \dfrac{\partial \boldsymbol{x}}{\partial \xi^\alpha}$. We therefore recast the isotropic 3D GMAC scheme as

The GMAC3Dc-iso Scheme:

Solve for $\boldsymbol{u} \in C^1\big([0,T]; L^2(\Omega_{\mathrm{c}}, \mathbb{R}^3)\big)$ and $p \in C^0\big([0,T]; L^2(\mathring{\Omega}_{\mathrm{g}}, \mathbb{R})\big)$ such that

$$\text{(B.19)} \qquad \begin{aligned} \boldsymbol{u}_t + \bar{\boldsymbol{\omega}} \times \boldsymbol{u} + \bar{\nabla}_h p &= -\nu \bar{\nabla}_h \times \boldsymbol{\omega} + \boldsymbol{f} & \text{on } \Omega_{\mathrm{c}} \\ \boldsymbol{\omega} &= \bar{\nabla}_h' \times \boldsymbol{u} & \text{on } \bar{\Omega}_{\mathrm{g}} \\ \bar{\nabla}_h' \cdot \boldsymbol{u} &= 0 & \text{on } \bar{\Omega}_{\mathrm{g}} \end{aligned}$$

with $\bar{\boldsymbol{\omega}} = (\bar{\omega}^1, \bar{\omega}^2, \bar{\omega}^3)$ and $\bar{\boldsymbol{\omega}} \times \boldsymbol{u} \in L^2(\Omega_{\mathrm{c}}, \mathbb{R}^3)$ defined by

$$\text{(B.20)} \qquad \bar{\boldsymbol{\omega}} \times \boldsymbol{u} := \sqrt{g_h} \begin{vmatrix} \boldsymbol{e}^1 & \boldsymbol{e}^2 & \boldsymbol{e}^3 \\ \bar{\omega}^1 & \bar{\omega}^2 & \bar{\omega}^3 \\ u^1 & u^2 & u^3 \end{vmatrix}, \qquad \bar{\omega}^\alpha := A_1 A_2 A_3 \omega^\alpha \in L^2(\Omega_{\mathrm{c}}, \mathbb{R}),$$

and

$$\text{(B.21)} \qquad \bar{\nabla}_h' \cdot : L^2(\Omega_{\mathrm{c}}, \mathbb{R}^3) \mapsto L^2(\bar{\Omega}_{\mathrm{g}}, \mathbb{R}), \qquad \bar{\nabla}_h' \cdot \boldsymbol{u} = \frac{1}{\sqrt{g_h}}\Big(\sum_{\alpha=1}^{3} \bar{D}_\alpha'(\sqrt{g_h} u^\alpha) \Big),$$

$$\text{(B.22)} \qquad \bar{\nabla}_h' \times : L^2(\Omega_{\mathrm{c}}, \mathbb{R}^3) \mapsto L^2(\bar{\Omega}_{\mathrm{g}}, \mathbb{R}^3), \qquad \bar{\nabla}_h' \times \boldsymbol{u} = \frac{1}{\sqrt{g_h}} \begin{vmatrix} \boldsymbol{e}_1 & \boldsymbol{e}_2 & \boldsymbol{e}_3 \\ \bar{D}_1' & \bar{D}_2' & \bar{D}_3' \\ u_1 & u_2 & u_3 \end{vmatrix},$$

$$\text{(B.23)} \qquad \bar{\nabla}_h \times : L^2(\bar{\Omega}_{\mathrm{g}}, \mathbb{R}^3) \mapsto L^2(\Omega_{\mathrm{c}}, \mathbb{R}^3), \qquad \bar{\nabla}_h \times \boldsymbol{\omega} = \frac{1}{\sqrt{g_h}} \begin{vmatrix} \boldsymbol{e}_1 & \boldsymbol{e}_2 & \boldsymbol{e}_3 \\ \bar{D}_1 & \bar{D}_2 & \bar{D}_3 \\ \omega_1 & \omega_2 & \omega_3 \end{vmatrix}.$$

It can be shown that analogue of (B.10) remains valid for the discrete operators $\bar{\nabla}'_h\cdot$, $\bar{\nabla}'_h\times$ and $\bar{\nabla}_h\times$ as well. In (B.20-B.23), the co-variant components and contra-variant components of a vector field $\boldsymbol{v}$ in $L^2(\Omega_c, \mathbb{R}^3)$ or $L^2(\bar{\Omega}_g, \mathbb{R}^3)$ are transformed to each other through

(B.24)
$$v^\mu = \sum_{\nu=1}^3 g_h^{\mu\nu} v_\nu \quad \text{and} \quad v_\mu = \sum_{\nu=1}^3 g_{\mu\nu}^h v^\nu$$

whenever necessary. Here $g_h^{\mu\nu}$ and $g_{\mu\nu}^h$ are (numerical) metric tensors with respect to the default coordinate (ξ^1, ξ^2, ξ^3) defined on cell centers and satisfy

$$\sum_{\gamma=1}^3 g_h^{\mu\gamma} g_{\gamma\nu}^h = \delta_\nu^\mu.$$

The corresponding isotropic Laplacian is given by

(B.25) $\qquad \bar{\triangle}'_h : L^2(\bar{\Omega}_g, \mathbb{R}) \mapsto L^2(\bar{\Omega}_g, \mathbb{R}), \qquad \bar{\triangle}'_h p = \bar{\nabla}'_h \cdot \bar{\nabla}_h p = \dfrac{1}{\sqrt{g_h}} \sum_{\mu,\nu=1}^3 \bar{D}'_\mu(\sqrt{g_h} g_h^{\mu\nu} \bar{D}_\nu p).$

The 3D analogue of Lemma 3.1 remains valid for the isotropic difference operators

LEMMA B.1. *For $\boldsymbol{u} \in L^2(\Omega_c, \mathbb{R}^3)$, $\boldsymbol{v} \in L^2(\bar{\Omega}_g, \mathbb{R}^3)$ and $p \in L^2(\bar{\Omega}_g, \mathbb{R})$, we have*

1.

(B.26)
$$\langle\, \boldsymbol{u}\,,\, \bar{\nabla}_h p \,\rangle_{\Omega_c} = -\langle\, \bar{\nabla}'_h \cdot \boldsymbol{u}\,,\, p \,\rangle_{\bar{\Omega}_g}$$

2.

(B.27)
$$\langle\, \boldsymbol{u}\,,\, \bar{\nabla}_h \times \boldsymbol{\omega} \,\rangle_{\Omega_c} = \langle\, \bar{\nabla}'_h \times \boldsymbol{u}\,,\, \boldsymbol{\omega} \,\rangle_{\bar{\Omega}_g}$$

3.

(B.28)
$$\bar{\triangle}'_h p = \bar{\nabla}'_h \cdot \bar{\nabla}_h p$$

4. *If $\boldsymbol{\psi} \in L^2(\bar{\Omega}_g, \mathbb{R}^3)$, then*

(B.29)
$$\bar{\nabla}'_h \cdot \bar{\nabla}_h \times \boldsymbol{\psi} \equiv 0 \quad \text{on } \mathring{\bar{\Omega}}_g.$$

If in addition, $\boldsymbol{\psi} \times \boldsymbol{n} = \boldsymbol{0}$ on Γ_g, then

(B.30)
$$\bar{\nabla}'_h \cdot \bar{\nabla}_h \times \boldsymbol{\psi} \equiv 0 \quad \text{on } \bar{\Omega}_g.$$